Extreme Optomechanically Induced Transparency

by

Timothy Paul Bodiya

Submitted to the Department of Physics
in partial fulfillment of the requirements for the degree of

Masters of Science in Physics

at the

MASSACHUSETTS INSTITUTE OF TECHNOLOGY

February 2015

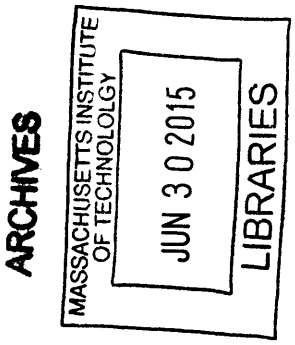

Signature redacted

Author .....

Department of Physics
February 9, 2015

Signature redacted

Certified by .....

Nergis Mavalvala
Curtis (1963) and Kathleen Marble Professor of Astrophysics
Thesis Supervisor

Signature redacted

Accepted by .....

Krishna Rajagopal
Associate Department Head for Education

Extreme Optomechanically Induced Transparency

by

Timothy Paul Bodiya

Submitted to the Department of Physics
on February 9, 2015 , in partial fulfillment of the
requirements for the degree of
Masters of Science in Physics

Abstract

This thesis describes the theory and experimental implementation optomechanically induced transparency utilizing ultra low loss mechanical oscillators and high laser power to achieve extremely strong optical induced transparency effects. This system modifies the light transmission properties of the optical cavity reducing the transmission by a factor of 3×10^{-3} at the highest power levels. A linewidth reduction of 5×10^{-5}, from 10 kHz to 20 mHz, has been achieved.

Thesis Supervisor: Nergis Mavalvala
Title: Curtis (1963) and Kathleen Marble Professor of Astrophysics

Acknowledgments

This thesis would not have been possible without the great support of many people. First and foremost I want to thank Nergis Mavalvala for her continued support and understanding over my whole career at MIT. Even if my career at MIT didn't end how I hoped or imagined, it was a great ride and she was a huge part of that.

The MIT LIGO Lab is a great place to work and everyone there contributes to a vibrant intellectual atmosphere. In particular, I want to single out the lab technician Myron Mcinnis, who provided invaluable support for all experimental work, our administrator Marie Woods, who saved me countless hours with her extreme helpfulness, and Fred Donovan, who was always ready to help out with the computer problems. They are the unsung heroes of the lab. I'd also like to thank Rich Mittleman, who was always willing to lend a hand when help was needed and look the other way when it wasn't.

This thesis was built upon the a great deal of work by both Thomas Corbitt and Christopher Wipf. The vast majority of my knowledge about interferometers and optomechanics comes from them. I can't thank them enough. Chris and I spent many long nights, going into days noise hunting and getting the interferometer to work. I'd like to thank Eric Oelker for the great photodetectors, and for trying to get us to work during the day and Abraham Neben for his contributions to the COMSOL modeling of our suspension.

My time at MIT was also made easier by sharing it with other fellow grad students and postdocs, Nic, Sheila, Tomoki, Lindy, Leo, Mike, Ben, Nancy, William, Adam, John, Adam, Slawek, Anna, Amelia the list goes on and I'm sure I forgot many names.

Finally, I'd like to thank all my friends, climbing partners, running buddies, for making the time to explore the Boston area outside of the lab. Most importantly of course, I want to thank my family and especially Yulan for their support and love. They make it all worthwhile.

Contents

List of Figures

List of Tables

Chapter 1

Introduction

There has recently been a large research effort and interest in coupling oscillating mechanical systems lasers [8, 12, 14, 28, 27, 15]. This interest is motivated by many things, one of which is the quest to observer quantum mechanical behavior of massive objects [18, 7]. To observe quantum mechanical effects in opto-mechanical systems the noises in the system must be lower than the quantum mechanical fluctuations. The dominant noises in the system arise from thermal noise of the mechanical oscillator. In the optical regime lasers have no thermal noise, T=0. This makes them a very clean way to actuate on the mechanical systems. In addition, by designing the optomechanical system in specific ways, you can engineer a variety of different effects that can probe disparate physical regimes.

Many of these experiments use an optical cavity to increase the interaction strength between light and the mechanical oscillator [8, 12, 14, 28, 27]. The simplest effect of the cavity is to amplify the number of times that a single photon will interact with the mechanical oscillator. In addition, the frequency shift between the cavity and the laser field allow for a variety of different energy exchanges to happen between the cavity and the mechanical oscillator. Much of the initial work has focused on how the optical field can modify the mechanical properties of oscillator [10, 11, 25, 14, 9]. For example, by detuning a laser to the blue (higher frequency) side of the cavity resonance, the optomechanical spring constant of the system can be dramatically increased. This effect is know as an optical spring [5, 19, 11, 9]. Systems exist where

the resonance frequency of the mechanical oscillator can be changed by orders of magnitude [11]. Detuning to the other side of the resonance, red detuning, will increase the optomechanical damping and can allow ground state cooling of the mechanical oscillator, referred to as cavity cooling [26, 6]. A combination of blue and red detuned fields can be used to create a stable optical trap for the mirror [10].

In addition, the dependence on cavity parameters, lock point of the opto-mechancial cavity system, and ability to engineer the oscillators allows experimenters to dynamically modify the response of the optomechanical system [5, 11, 19].

1.1 Electromagnetic vs optomechanically induced transparency

Instead of focusing on how the mechanical system can be modified by the optics, here we will focus on how the mechanical system can affect the optical properties of the optomechanical system. Specifically, we will focus on how the optical cavity linewidth can be dramatically narrowed due to its interaction with the mechanical oscillator. This is very similar to the phenomenom of electromagnetically induced transparency (EIT) where a strong laser field changes the absorption properties of an atomic system [13, 4]. The optomechanical analogue of EIT is referred to as optomechanically induced transparency (OMIT) [1].

Unlike EIT, where the atomic system in question is fixed by nature, an optomechanical system can be engineered for a specific application. In EIT, the losses and frequencies of the system are intrinsic to the atomic transitions used, but in the optomechanical systems these are free design parameters. In addition, as we will see in the following chapters, the optomechanical interaction can be made incredibly strong, which is one of the limitations of EIT. While not impossible, EIT experiments struggle to achieve optical depths of greater than 0.5. The first OMIT experiments achieved dips on the order of $\frac{1}{100}$ and in this thesis we will see data showing dips of great than $\frac{1}{1000}$ [30, 23].

Another key difference between the experiment described here and previous work [30, 23] is that we have achieved large OMIT effects while operating at room temperature. Because our system can handle much higher power, we use this feature to overcome the excess mechanical loss that room temperature operation brings. In the first OMIT experiments by the Painter group [23], they struggled to achieve a cooperativity of 1 at room temperature. Here we will show cooperativities of almost 50 at room temperature.

1.2 Application so systems with controllable transparency

OMIT and EIT can be used for optical information storage, by changing the cavity storage time dynamically. This offers exciting possibilities for compact systems that can have long storage times. There is a tradeoff in bandwidth and storage time however, known as the bandwidth-delay limit [2]. It essentially says that it is not possible to have a system with infinite bandwidth and infinite delay. The combination of the two is finite. The intial systems that demonstrated OMIT operated in the MHz regime resulting in storage times, equivalent to OMIT linewidth, in the microsecond regime. In this thesis we will be describing a system and showing measurements of an OMIT feature that would enable storage times on the scale of hours, corresponding to a linewidth of approximately 20 mHz.

This extremely long storage time also allows for this system to be used in place of an optical cavity with a small linewidth. Two uses for this are filter cavities for gravitational wave detection [17] and optical frequency stabilization [16]. Achieving very low linewidths along with the ability to dynamically change the optical properties of the system opens up other avenues. One such possibility might be tracking an inspiralling neutron star by changing the filter cavity parameters in a gravitational wave detector.

Chapter 2 describes the theory of radiation pressure and optomechanically induced

transparency using the Langevin equation formalism. In addition, some simple control theory concepts are discussed which will be used later in chapter four.

Chapter 3 describes the experimental setup, focusing on the unique features of our system that enable the ultra-low mechanical linewidth, the small cavity linewidth, and the extremely high power operation at room temperature.

Chapter 4 describes experimental measurements of optomechanically induced transparency on the apparatus of Chapter 3.

Chapter 5 discusses possible uses of the OMIT system described here and limitations to the current setup.

Chapter 2

Theory

In this chapter we will develop the theoretical underpinnings necessary for the rest of the thesis. In Figure 2-1 is a plot of the mechanical oscillator and cavity system that we will be theoretically describing in the rest of the chapter.

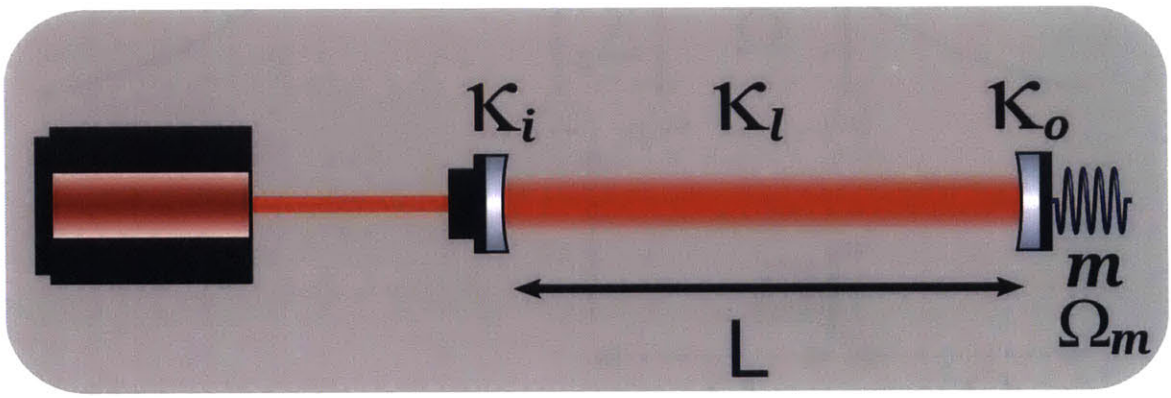

Figure 2-1: A Fabry-Perot cavity with a moveable mirror. The length of the cavity is L meters, the intra-cavity power loss is κ_l, the input mirror power transmission is κ_i, and the output mirror (M_o) is κ_o. $\kappa_{tot} = \sum \kappa_x$ The compliant mechanical oscillator has a mass of m kg, and a resonance frequency of $\frac{\Omega_m}{2\pi}$ Hz.

In OMIT, a strong control field (optimally red-detuned to the mechanical resonance frequency) will mediate interactions between another weaker probe field and the mechanical oscillator. This interaction can dramatically change the cavity transmission and reflection properties. The basic scenario is that the beat between the control field and the probe field causes radiation pressure induced oscillations of the mechanical resonator. Then since the cavity is detuned, there is an asymmetric re-

sponse of the upper and lower mechanical sideband inside of the cavity. This creates a feedback loop which then can interfere with the probe field depending on certain conditions. To see this we will analyze the optomechanical Hamiltonian to solve for the fields inside of the cavity in the presence of the strong control field. See Figure 2-2 for a plot of the relevent frequencies and variables.

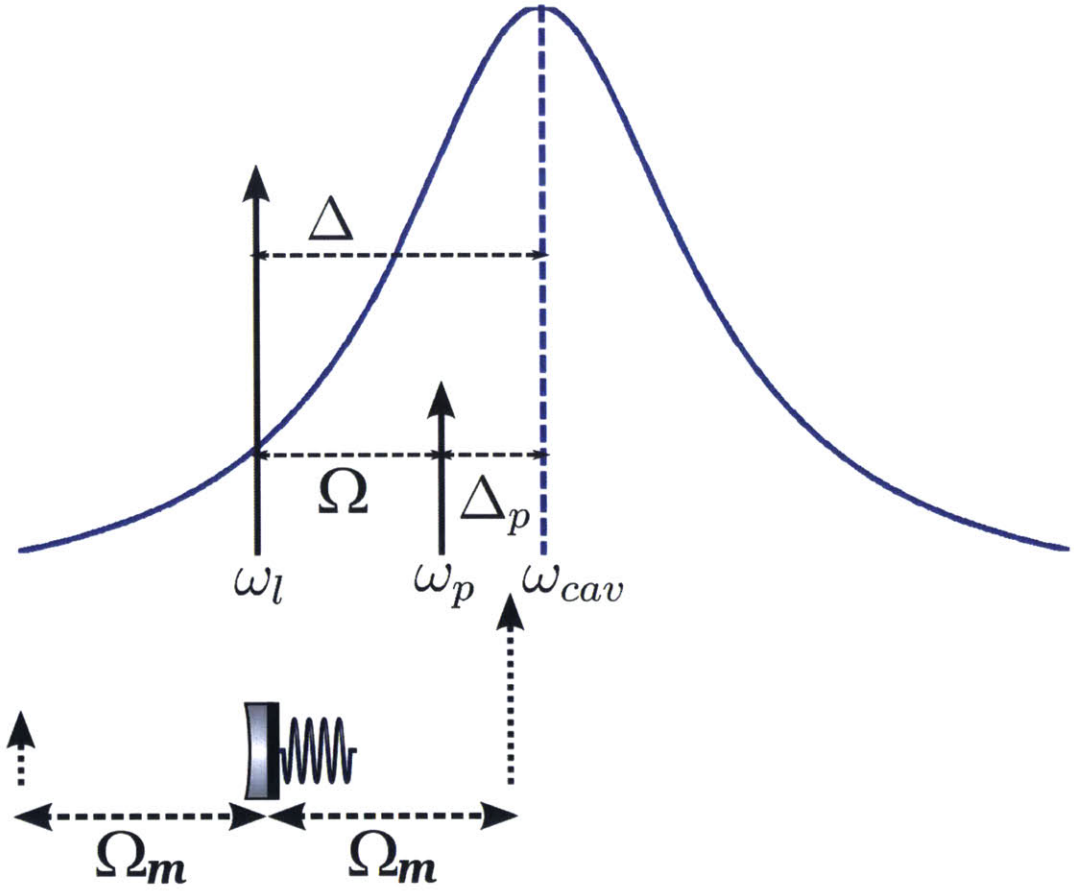

Figure 2-2: A plot of the relevant frequencies when observing OMIT. The blue curve represents the cavity resonant field. A control laser at frequency, ω_l, is detuned from the cavity resonance, ω_{cav}, by an amount, Δ. In the optimal case, $\Delta = -\Omega_m$. A probe laser at frequency, $\omega_p = \omega_l + \Omega$, is launched into the cavity. To see the strongest response, the probe would be on resonant with the cavity mode, $\Delta_p = 0$.

2.1 Definitions

In the chapter we will use a variety of different variables which are summarized in Table 2.1.

Symbol	Parameter/Equation	Units/Value
ω_{cav}	Cavity Resonance Frequency	$\frac{rad}{s}$
ω_l	Laser Frequency	$\frac{rad}{s}$
G	Bare Optomechanical Coupling Constant ($\frac{\omega_{cav}}{L}$)	$\frac{rad}{s*m}$
$s_{in}(t)$	Input Laser Field ($(\bar{s_{in}} + \delta s_{in}(t))e^{-i\omega_l t}$)	$\sqrt{\text{photon number}}$
$\bar{s_{in}}$	Average laser field	$\sqrt{\text{photon number}}$
$\delta s_{in}(t)$	Modulation to laser field	$\sqrt{\text{photon number}}$
Δ	Control Field Detuning, $\omega_l - \omega_{cav}$	$\frac{rad}{s}$
Δ_p	Probe Detuning, $\Delta + \Omega$	$\frac{rad}{s}$
κ_o	Output Loss Rate (Power)	$\frac{rad}{s}$
$\frac{\kappa_i}{2\pi}$	Input Loss Rate (Power)	$\frac{rad}{s}$
$\frac{\kappa_l}{2\pi}$	Cavity Loss Rate (Power)	$\frac{rad}{s}$
L	Cavity Length	meter
w_0	Cavity Waist	meters
m	Resonator modal mass	kg
Ω_m	Mechanical Resonance Frequency	$\frac{rad}{s}$
Γ_m	Mechanical Damping Rate	$\frac{rad}{s}$
$\hat{p}$	Momentum Operator for Resonator	$\frac{meters}{seconds}$
$\hat{x}$	Position Operator for Resonator	meters
$\hbar$	Reduced Planck Constant	
$\hat{a}$	Cavity photon annihilation operator	$\sqrt{\text{photon number}}$
$\hat{a}^\dagger$	Cavity photon creation operator	$\sqrt{\text{photon number}}$
$\bar{a}$	Square root of mean number of cavity photons	$\sqrt{\text{photon number}}$
A_-	Upper Cavity Sideband ansatz	$\sqrt{\text{photon number}}$
A_+	Lower Cavity Sideband ansatz	$\sqrt{\text{photon number}}$
Ω	Cavity Sideband Frequency	$\frac{rad}{s}$
$\chi(\Omega)$	Mechanical Susceptibility, $\frac{1}{m(\Omega_m^2 - i\Omega\Gamma_m - \Omega^2)}$	
$z(\Omega)$	$\frac{\hbar G^2 \lvert\bar{a}\rvert^2 \chi(\Omega)}{i(\Delta - \Omega) + \frac{\kappa_t}{2}}$	

Table 2.1: Parameters and variables used in the following chapter.

2.2 Mathematical Formulation of OMIT

Here we will use the Heisenberg equations [24] to derive the behavior of the optomechanical system. For some variable A_i, it will obey equation 2.1.

$$\frac{dA_i}{dt} = \frac{i}{\hbar}[H_{sys}, A_i] \tag{2.1}$$

The Hamiltonian that will be used is for the system of a mechanical oscillator coupled to an optical cavity. For an optical cavity with frequency ω_{cav}, coupled to a mechanical oscillator, with mass m, and resonance frequency Ω_m, pumped by a laser with frequency ω_l, we have the Hamiltonian, $H_{tot} = H_{OM} + H_l$. The optomechanical Hamiltonian, H_{OM}, is:

$$H_{OM} = \underbrace{\hbar\omega_{cav}(\hat{a^\dagger}\hat{a} + \frac{1}{2})}_{\text{cavity}} + \underbrace{\frac{\hat{p}^2}{2m} + \frac{1}{2}m\Omega_m\hat{x}^2}_{\text{mechanics}} + \underbrace{\hbar G\hat{x}\hat{a}^\dagger\hat{a}}_{\text{interaction}} \tag{2.2}$$

$\hat{a}^\dagger$ and $\hat{a}$ are the creation and annihilation operators for the cavity photons. $\hat{x}$ and $\hat{p}$ are the position and momentum operators for the mechanical oscillator that has a modal mass, m, and a resonance frequency of Ω_m. $G = \frac{\omega_{cav}}{L}$ is the single photon optomechanical coupling constant. It describes how the quantum zero point fluctuations change the cavity mode . To see how this coupling arises we will follow the simple derivation due to Pace, Collet and Walls[20].

The Hamiltonian of the fixed cavity is:

$$H_{cav} = \hbar\omega_{cav}\hat{a}^\dagger\hat{a} \tag{2.3}$$

where $\omega_{cav} = \frac{n\pi c}{L}$. If the cavity mirror moves from position L to $L+x$, then the cavity frequency also changes, which modifies the Hamiltonian:

$$H'_{cav} = \hbar\frac{n\pi c}{L+x}\hat{a}^\dagger\hat{a} \tag{2.4}$$

$$\approx \hbar\omega_{cav}(1-\frac{x}{L})\hat{a}^\dagger\hat{a} \tag{2.5}$$

$$= H_{cav} - \hbar\omega_{cav}\frac{x}{L}\hat{a}^\dagger\hat{a} \tag{2.6}$$

Comparing to equation 2.2, G is defined as $\frac{\omega_{cav}}{L}$

Added to the basic optomechanical Hamiltonian is a driving force from a laser with $s_{in}(t)$ representing the input laser field in units of $\sqrt{\text{photons}}/s$.

$$H_l = i\hbar\sqrt{\kappa_i}(s_{in}(t)\hat{a^\dagger} - s^*_{in}(t)\hat{a}) \tag{2.7}$$

$$s_{in}(t) = (\bar{s_{in}} + \delta s_{in}(t))e^{-i\omega_l t} \tag{2.8}$$

The Heisenberg equations for this system then take the form:

$$\frac{d\hat{a}}{dt} = (i\Delta - \frac{\kappa_{tot}}{2})\hat{a} - iG\hat{x}\hat{a} + \sqrt{\kappa_i}s_{in} \tag{2.9}$$

$$\frac{d\hat{x}}{dt} = \frac{\hat{p}}{m} \tag{2.10}$$

$$\frac{d\hat{p}}{dt} = -m\Omega_m^2\hat{x} - \hbar G\hat{a}^\dagger\hat{a} - \Gamma_m\hat{p} \tag{2.11}$$

At DC this gives coupled equations between $\bar{\hat{a}}$ and $\bar{\hat{x}}$. From here on we will neglect the hat operator symbol so as not to cause confusion with the bar of the average values:

$$\bar{a} = \frac{\sqrt{\kappa_i}\bar{s_{in}}}{-i(\Delta - G\bar{x}) + \frac{\kappa_{tot}}{2}} \tag{2.12}$$

$$\bar{x} = \frac{\hbar G\bar{a}^2}{m\Omega_m^2} \tag{2.13}$$

From equation 2.13, we see that the radiation pressure of the cavity field causes the

mechanical oscillator to move by an amount

$$\frac{\hbar G\bar{a}^2}{m\Omega_m^2}$$

.

It should be noted that the coupled equations above are in the absence of any cavity control. A control system will allow for the equations to be decoupled, for example by applying a force to the mechanical oscillator or changing the laser frequency to stay on resonance.

To gain more insight, the next step is to linearize the equations, so $\vartheta = \bar{\vartheta} + \delta\vartheta$. Equations 2.9 to 2.11, become:

$$\frac{d}{dt}\delta a = (i\bar{\Delta} - \frac{\kappa_{tot}}{2})\delta a - iG\bar{a}\delta x + \sqrt{\kappa_i}\delta s_{in} \tag{2.14}$$

$$\frac{d^2\delta x}{dt^2} + \Gamma_m\frac{d\delta x}{dt} + \Omega_m^2\delta x = \frac{-\hbar G}{m}(\bar{a}^*\delta a + \bar{a}\delta a^\dagger) \tag{2.15}$$

To solve these equations, we first make the following ansatz for the cavity field and the mechanical oscillator:

$$\delta s_{in} = s_+e^{-i\Omega t} + s_-e^{-i\Omega t} \tag{2.16}$$

$$\delta a = A_-e^{-i\Omega t} + A_+e^{i\Omega t} \tag{2.17}$$

$$\delta a^\dagger = A_-^*e^{i\Omega t} + A_+^*e^{-i\Omega t} \tag{2.18}$$

$$\delta x = Xe^{-i\Omega t} + X^*e^{i\Omega t} \tag{2.19}$$

Using the the ansatz in equations 2.14 to 2.15 gives the follwing equations

$$(-i(\Omega+\bar{\Delta})+\frac{\kappa_{tot}}{2})A_- = -iG\bar{a}X+\sqrt{\kappa_i}s_- \tag{2.20}$$

$$(-i(-\Omega+\bar{\Delta})+\frac{\kappa_{tot}}{2})A_+ = -iG\bar{a}X^*-\sqrt{\kappa_i}s_+ \tag{2.21}$$

$$m(\Omega_m^2-i\Omega\Gamma_m-\Omega^2)X = -\hbar G(\bar{a}^*A_- + \bar{a}A_+^*) \tag{2.22}$$

with the standard definition of mechanical susceptiblility, $\chi(\Omega) = \frac{1}{m(\Omega_m^2-i\Omega\Gamma_m-\Omega^2)}$. Using equations 2.20-2.22 we can then solve for A_-, A_+^*, which then gives us X.

$$A_- = \frac{\sqrt{\kappa_i}}{-i(\Delta+\Omega)+\frac{\kappa_t}{2}+2\Delta z(\Omega)}\left(iz(\Omega)\frac{\bar{a}}{\bar{a}^*}s_-^* + \{(1+iz(\Omega)\}s_+\right) \tag{2.23}$$

$$A_+^* = -i\frac{\bar{a}^*}{\bar{a}}\frac{z(\Omega)}{1+iz(\Omega)}A_- + \frac{\sqrt{\kappa_i}}{(1+iz(\Omega))(i(\Delta-\Omega)+\frac{\kappa_t}{2})}s_-^* \tag{2.24}$$

where we have defined

$$z(\Omega) = \frac{\hbar G^2|\bar{a}|^2\chi(\Omega)}{i(\bar{\Delta}-\Omega)+\frac{\kappa_t}{2}}$$

. As will be seen in Section 2.2.2, all of the dynamics of OMIT are contained within z(Ω).

2.2.1 Transmitted Light Signal

Here we will focus on detecting the signals via the transmitted light through the cavity. Using the input-output relations, the field incident on the transmitted light photodetector is [29]:

$$s_{out}(\Omega) = \sqrt{\kappa_o}a(t) \tag{2.25}$$

$$= e^{-i\omega_l t}\sqrt{\kappa_o}(\bar{a}+A_-e^{-i\Omega t}+A_+e^{i\Omega t}) \tag{2.26}$$

The photodetector measures power, so the signal is:

$$|s_{out}|^2 = \text{DC terms} + \kappa_o\big((\bar{a}A_+^* + \bar{a}^*A_-)e^{-i\Omega t} + (\bar{a}A_-^* + \bar{a}^*A_+)e^{i\Omega t}\big) + 2\ \Omega \text{ terms} \tag{2.27}$$

We are interested in the signal oscillating at sideband frequency Ω, which is

$$|s_{out}|^2 = \bar{a}A_+^* + \bar{a}^*A_-$$

2.2.2 A limiting case

First, we will operate under three assumptions to derive the OMIT signal:

- There is a control field with amplitude $\bar{a}$ at frequency ω_l detuned from the cavity frequency by amount Δ.
- There is a weaker control field, represented by $\delta s_{in} = s_+ e^{-i\Omega t}$ at frequency $\omega_l + \Omega$ which is detuned from the cavity by an amount Δ_p.
- We are in the resolved sideband regime, $\Omega_m > \kappa_{tot}$, so that we can neglect the lower sideband, A_+ from the following discussion.

With these assumptions, we then have the following for A_:

$$A_- = \frac{\sqrt{\kappa_i}}{-i(\Delta + \Omega) + \frac{\kappa_t}{2} + 2\Delta z(\Omega)}\big(1 + iz(\Omega)\big)s_+ \tag{2.28}$$

The first limit to consider is when the OMIT feature does not exist at all. This corresponds to the case when there is no radiation pressure coupling from the oscillator to the cavity. One way to see this is to let the mass of the oscillator become infinite or for the control power to go to zero, $\bar{a} = 0$. In this limit, we obtain:

$$\chi(\Omega) = \frac{1}{m(\Omega_m^2 - i\Omega\Gamma_m - \Omega^2)} \to 0 \tag{2.29}$$

$$z(\Omega) = \frac{\hbar G^2 |\bar{a}|^2 \chi(\Omega)}{i(\bar{\Delta} - \Omega) + \frac{\kappa_t}{2}} \to 0 \tag{2.30}$$

$$A_- = \frac{\sqrt{\kappa_i}}{-i(\Delta + \Omega) + \frac{\kappa_t}{2}} s_+ \tag{2.31}$$

Equation 2.31 for A_- is just the standard effect that a cavity has on some input field, s_+. Also, note that the magnitude of $z(\Omega)$ is tunable by varying the control field while the can be changed by the various field detunings. The $z(\Omega)$ terms are what contain the dynamics of the interference that causes drastic change in the cavity transmission. In Figures 2-3 and 2-4 are plots showing how the cavity tranmission is

changed with a control field of 1 Watt, $\Delta = -\Omega_m$, $Q = 1.1{\times}10^6$, $m = 125$ grams, $\frac{\kappa_{tot}}{2\pi} \approx 10$ kHz, and $G = 1.7 \times 10^{15}$.

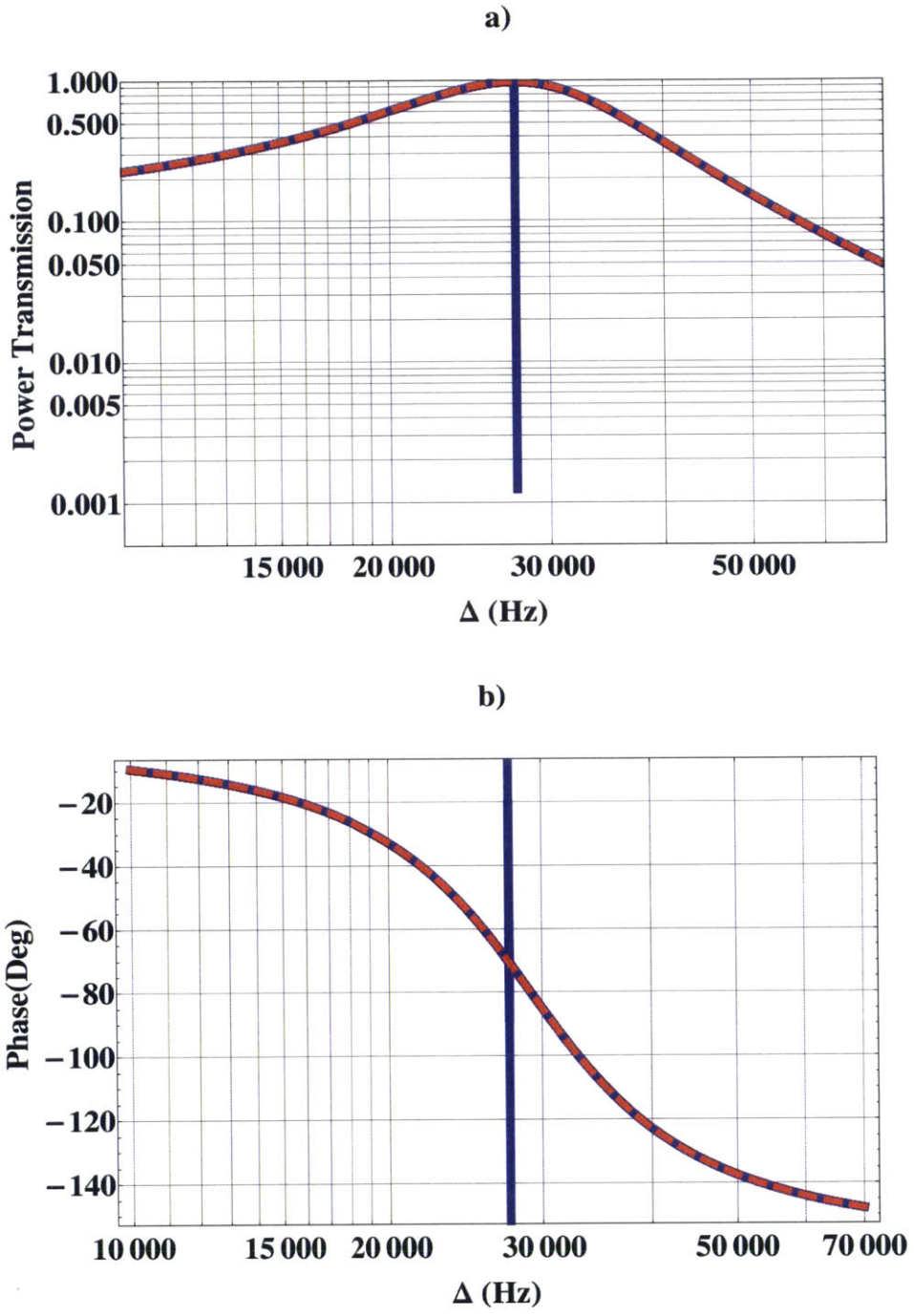

Figure 2-3: A wideband Bode plot of the transfer function of the transmitted light of the probe field relative to the input field. The red trace is when there is no OMIT feature, $m \to \infty$. The blue trace is with a mass of 0.125 kg. **a)** The transmitted light power of the probe field (scaled to a maximum of 1) and **b)** The phase of the transfer function. This plot uses an input control field power of 1W, an oscillator mass of 0.125 kg, a resonance frequency $\frac{\Omega_m}{2\pi}$ of 27.5 kHz, and a quality factor of $Q = 1.1 \times 10^6$.

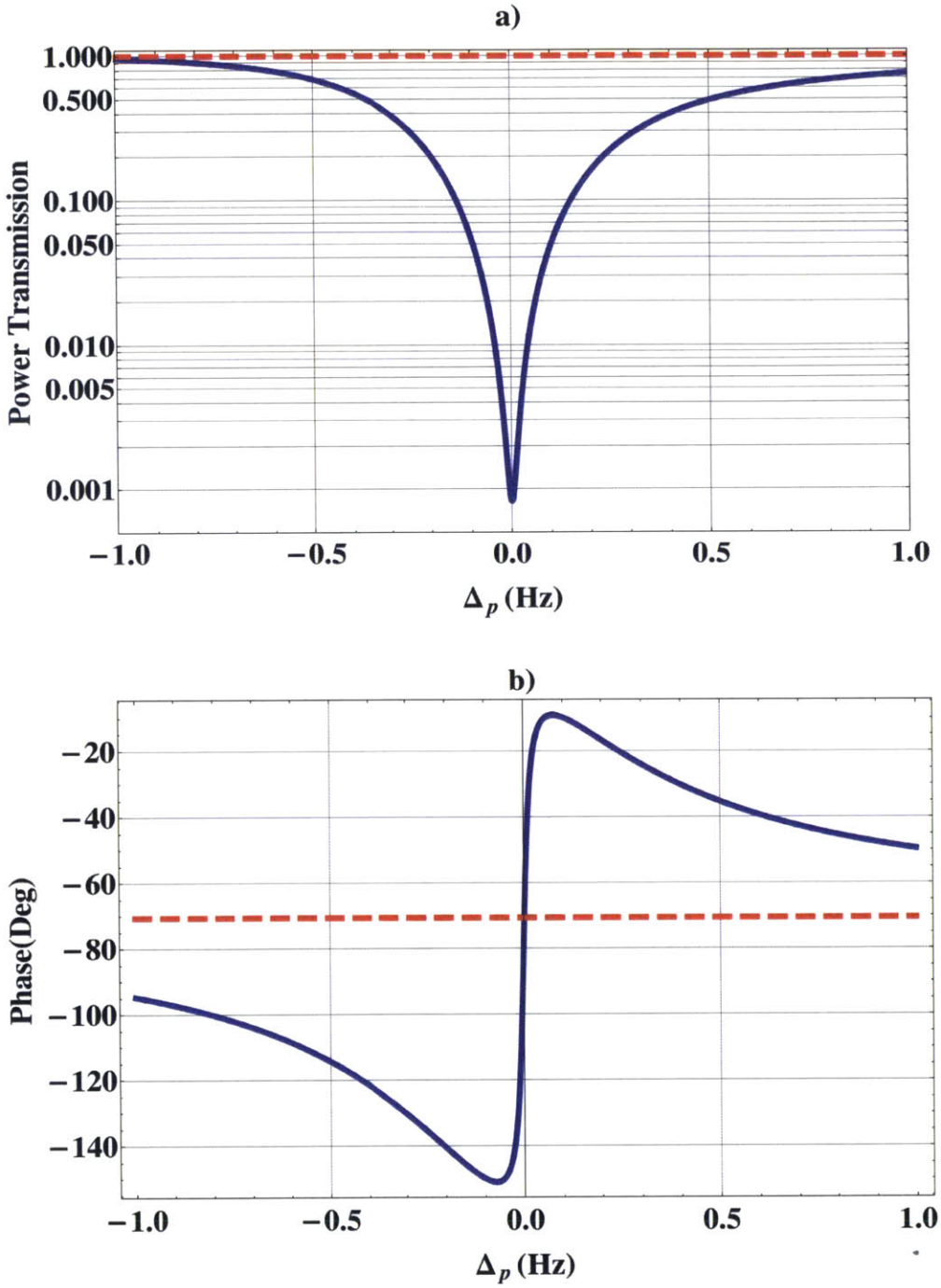

Figure 2-4: A narrowband Bode plot of the transfer function of the transmitted light of the probe field relative to the input field. The red trace is then there is no OMIT feature, $m \to \infty$. The blue trace is with a mass of 0.125 kg. **a)** The transmitted light power, t^2_{omit} (see Equation 2.35 and **b)** The phase of the transfer function. This plot uses an input control field power of 1W, an oscillator mass of 0.125 kg, a resonance frequency $\frac{\Omega_m}{2\pi}$ of 27.5 kHz, and a quality factor of $Q = 1.1 \times 10^6$.

For the largest OMIT dip, the control laser should be red-detuned from the cavity by the mechanical resonance frequency, $\Delta = -\Omega_m$. In addition, the probe beam will experience the greatest dip when it is on resonance with the cavity, $\Delta_p = 0$. With $\Delta = -\Omega_m$ this corresponds to $\Omega = \Omega_m$ and also implies that $s_- = 0$. Refer again to Figure 2-2. In addition, since we assume that we are in the resolved sideband regime, $\Omega_m > \kappa_{tot}$, we can neglect the lower sideband, A_+ from the following discussion. Then equations 2.20 and 2.22 simplify to, $\chi(\Omega) \approx -m\Omega_m(2\Delta_p + i\Gamma_m)$, where $\Delta_p = (\Omega - \Omega_m)$:

$$(i\Delta_p + \frac{\kappa_{tot}}{2})A_- = -iG\bar{a}X + \sqrt{\kappa_i}s_- \tag{2.32}$$

$$m\Omega_m(2\Delta_p - i\Gamma_m) = \hbar G\bar{a}^* A_- \tag{2.33}$$

which gives:

$$A_- = \frac{\sqrt{\kappa_i}s_-}{i\Delta_p + \frac{\kappa_{tot}}{2} + \frac{i\hbar G^2|\bar{a}|^2}{m\Omega_m(2\Delta_p - i\Gamma_m)}} \tag{2.34}$$

which gives the following for the ratio of probe field amplitude transmission with OMIT to the transmission of the probe field with no OMIT:

$$t_{omit} = \frac{A_-(\Delta_p = 0)}{A_-(\bar{a} = 0)} = \frac{1}{1 + \frac{2\hbar G^2|\bar{a}|^2}{m\Omega_m\Gamma_m\kappa_{tot}}} \tag{2.35}$$

Following the literature, we define the cooperativity C below. The cooperativity describes the relationship between the optomechanical coupling, and the losses in the system. When $C > 1$, the coupling has exceeded the system losses:

$$C = \frac{2\hbar G^2|\bar{a}|^2}{m\Omega_m\Gamma_m\kappa_{tot}} \tag{2.36}$$

Which gives the amplitude transmission of the cavity field as:

$$t_{omit} = \frac{1}{1 + C} \tag{2.37}$$

In addition, from Equation 2.34 we can find the width of the OMIT feature which is:

$$\Gamma_{OMIT} = C\Gamma_m \tag{2.38}$$

2.3 EIT vs OMIT

The phenomenon of electromagnetically induced transparency (EIT) in atomic systems is a very close analog of OMIT. In Figure 2-5 is a diagram of the energy level structure for EIT and OMIT. In both cases, a strong control laser couples two modes of the system. One mode of the system, $|2\rangle$ for EIT and $|b\rangle$ (the mechanical mode) for OMIT, is dark when the control field is off. In the case without any control field, the losses in the system are Γ_3 for EIT and κ_{tot} for OMIT. These losses define the response of the system to the probe field.

When the control field is present, it couples $|3\rangle \rightarrow |2\rangle$ and $|a\rangle \rightarrow |b\rangle$ for EIT and OMIT ,respectively. Now when the system is probed there are multiple decay pathways available. For EIT the basic pathways are **3→1** and **3→2→3→1**. In situatiosn with no dephasing loss, this would result in a completely transparent atomic system. The limit on the transparency is given by the dephasing of state 2, γ_{21}. In OMIT, there is a similar situation. A photon can decay from **a→optical bath** or **a→b→a→ optical bath**. Here the limit is set by the mechanical loss rate Γ_m which breaks the second decay channel with **a→b→mechanical bath**.

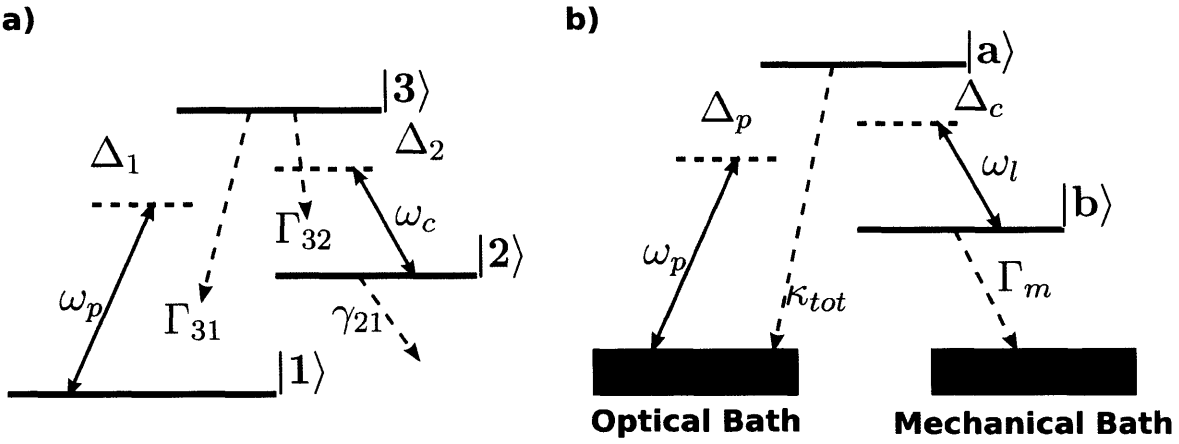

Figure 2-5: **a)** A diagram of the atomic level structure that allow for EIT. A control laser, at ω_c, couples level 2 and 3 of the atom. This allows for population to swap from level 3 to level 2. The 2→1 transition is forbidden. A probe beam interrogates the atom(s), at frequency ω_p. The spontaneous emission rates are Γ_{32} and Γ_{31} . In addition to the spontaneous emission, each level has a coherence dephasing rate given by γ_{ij}. **b)** A diagram of the analogous OMIT level structure. A control laser at ω_l pumps the cavity, coupling the mechanical ($|b\rangle$) and cavity ($|a\rangle$) modes. A probe laser then interrogates the system at frequency ω_p. The cavity field has a decay rate of κ_{tot}, and the mechanical oscillator a decay rate of Γ_m.

2.4 Control Theory

In our measurement of OMIT, as in many situations, the principles of measurement and feedback to allow the study of a system around a particular point of interest. In the following section, some basics of control theory needed in subsequent chapters will be reviewed. We restrict ourselves to linear, time-invariant control theory and work exclusively in the frequency domain.

2.4.1 Transfer Function

Given some component, be it an electrical circuit, a mechanical object, or something more complicated, we can define a transfer function as the response of the system to

an input:

$$R(\Omega) = H(\Omega)I(\Omega) \tag{2.39}$$

where $R(\Omega)$ is the response of the system at a specific frequency Ω, $I(\Omega)$ is the input applied to the system at frequency Ω, and $H(\Omega)$ is the transfer function that maps inputs to outputs.

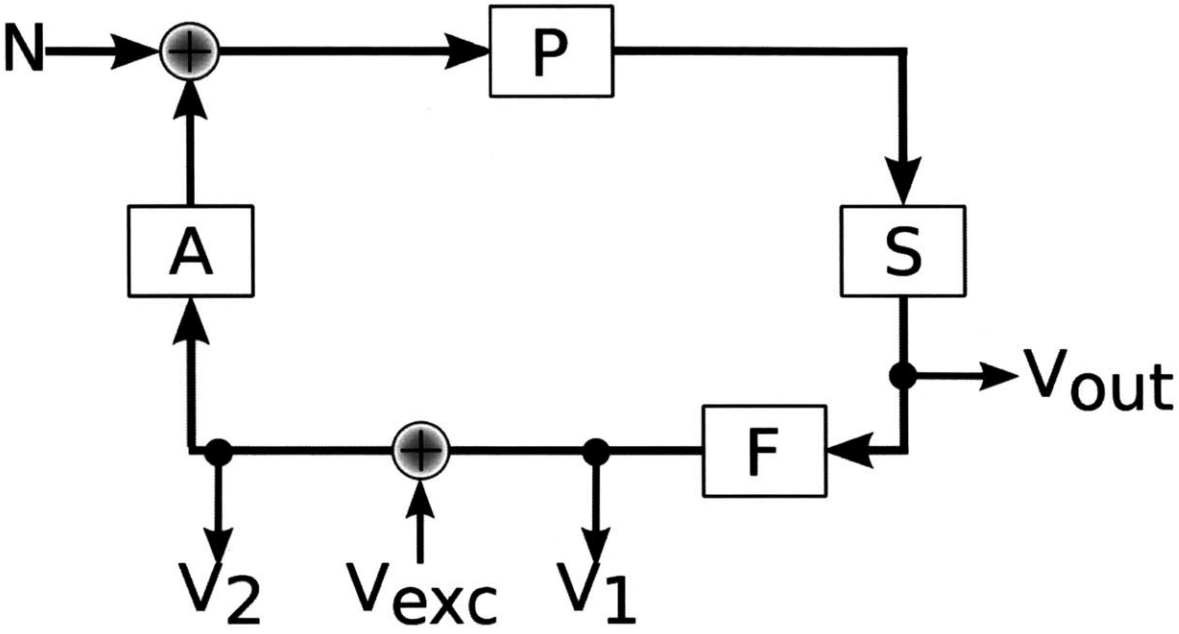

Figure 2-6: A simple block diagram with the plant (P), sensor (S), filter (F), and actuator (A), with noise, N, on the plant. Excitation V_{exc} is applied to the system. The plant is measured at V_{out}. The system can also be measured at points V_1 and V_2.

2.4.2 Components of a Control System

The basic components of a control system are the **Plant**, **Sensor**, **Actuator**, and control **Filter**. This is commonly drawn as the block diagram shown in Figure 2-6. The plant usually refers to the system that we wish to controll, denoted as P in the block diagram. The sensor provides information about the plant via a measurement process, denoted as S. This information is then fed into a filter, F, that changes the frequency content of the signal, amplifying some frequency bands and deamplifying

others. This component is crucial for ensuring loop stability. The signal from the filter is sent to an actuator, A, that applies this signal to the plant. In general, the control loop can have multiple filters, plants, sensors and actuators given by F_i, P_i, S_i, and A_i which are all functions of frequency.

With no feedback and no excitation ($V_{exc} = 0$), the signal measured at V_{out} in Figure 2-6 is:

$$V_{out} = N \cdot P \cdot S \tag{2.40}$$

which is the noise N filtered by the plant P and sensor S transfer functions.

If the feedback is engaged but V_{exc} still 0, then the situation is a bit more complicated. Now traversing the loop we see that:

$$(V_{out} \cdot F \cdot A + N) \cdot P \cdot S = V_{out} \tag{2.41}$$

which gives:

$$V_{out} = \frac{N \cdot P \cdot S}{1 - G} \tag{2.42}$$

where $G = F \cdot S \cdot F \cdot A$ is the open loop gain of the system. Comparing equation 2.40 to 2.42 shows that the output from the plant is suppressed by

$$\frac{1}{1 - G}$$

.

2.4.3 Measuring a transfer function

Many times it is desirable to know the transfer function of the different components of the system that we are interested in controlling so that we can create an optimal control filter. For A and S this is usually quite simple, F we will design, as an electronic or digital circuit, so this is also relatively easy. Unfortunately, the plant P, in its uncontrolled state is usually quite difficult to measure. This is why we are

building the control system after all. As long as the system is controlled (locked) to a reasonable degree the best way forward is to input a controlled excitation into the system and then measure the response to the excitation. Now with $V_{exc} \neq 0$, traversing the loop gives:

$$((V_1 + V_{exc})A + N)PSF = V_1 \tag{2.43}$$

$$(V_2 A + N)PSF + V_{exc} = V_2 \tag{2.44}$$

Combining these equations and assuming that V_{exc} is much larger than the noise, N, gives:

$$\frac{V_1}{V_2} = \frac{V_{exc}G + N \cdot PSF}{V_{exc} + N \cdot PSF} \approx G \tag{2.45}$$

By exciting the system with a drive at V_{exc} and measuring at V_1 and V_2, we can find the gain of the total system, G. If the component transfer functions, S, F, and A, are known this allows one to extract the plant transfer function P.

Chapter 3

Experimental Setup

Optomechanically induced transparency relies on the coupling between a cavity and a mechanical oscillator to allow radiation pressure to modify the cavity's optical response. In this chapter we will detail the main features of the experimental system, the optical cavity, the mechanical oscillator (which is part of the optical cavity), the laser system that pumps the cavity and mediates the interaction, and the experimental sensing and control systems that allow us to see the optomechanical effects.

Our system is a 1 meter long Fabry-Perot cavity consisting of two high reflectivity mirrors suspended as pendulums. In Figure 3-1 is a top level schematic of the experimental setup.

3.1 Laser System

In Figure 3-2 is a schematic of the pre-stabilized laser (PSL) system [21]. The PSL consists of a approxmately 10 W Lightwave MOPA (Master Oscillator Power Amplifier) laser operating at 1064 nm that is both intensity and frequency stabilized [21]. In addition, before any active stabilization, the laser beam is passed through a triangular ring cavity, called the pre-modecleaner (PMC), for the purposes of selecting a single TEM_{00} spatial mode and providing some very slight frequency noise suppression at higher frequencies. After the PMC part of the laser beam is split off to provide a signal for the intensity stabilization servo (ISS) that controls the relative intensity

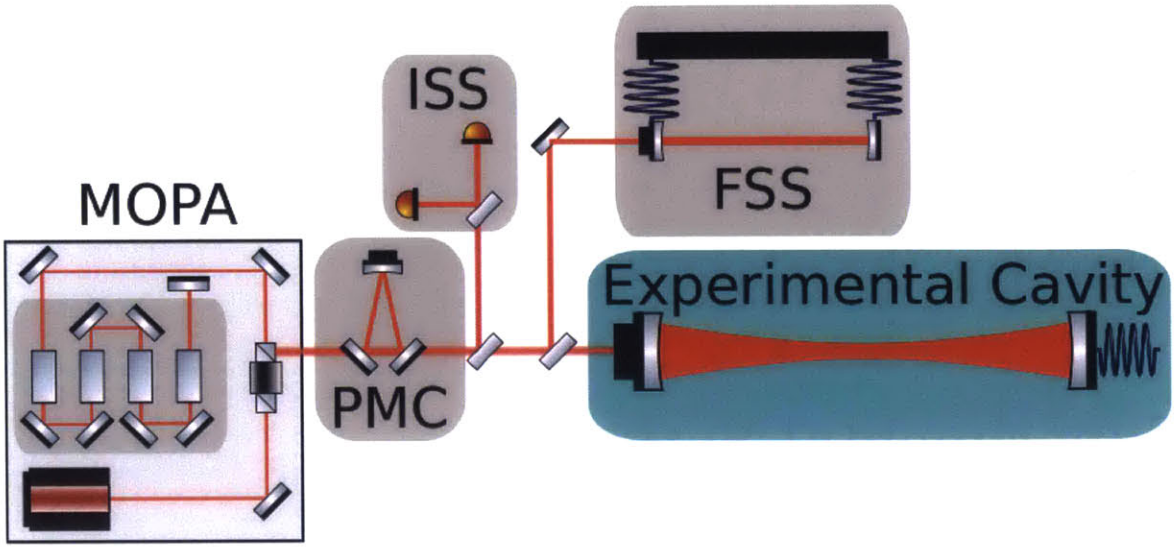

Figure 3-1: Schematic of the experiment. A 10 W laser beam with a wavelength of 1064 nm is transmitted through the pre-mode cleaner (PMC) cavity to provide spatial mode filtering and frequency stabilization at high frequencies. A pickoff provides light to lock the laser to a suspended reference cavity which provides frequency stabilization. This frequency stabilization system is referred to as the FSS. The light then enters the experimental cavity and interacts with the mechanical oscillator. Blue shading denotes that the cavity is in vacuum.

noise (RIN), down to a level of approximately 10^{-8}[22]. Another pickoff sends light to the reference cavity to provide frequency stabilization. Before the light enters the reference cavity, it is frequency shifted by an acoustooptic modulation (AOM), that allows the lockpoint of the FSS to be shifted. This provides high frequency length control of the experimental cavity.

The Frequency Stabilization System (FSS)

The frequency stabilization system (FSS) subsystem of the PSL is shown in more detail in Figure 3-3. The FSS servo locks the laser frequency to the length of the reference cavity. A pickoff from the main laser beam is double passed through an 80 MHz AOM (160 MHz total offset) driven by a voltage controlled oscillator (VCO) and then passed through an EOM that provides RF sidebands to lock the pickoff beam to the reference cavity. The signal from PD3 is sent to a tabletop FSS board (D040105) that demodulates the signal, filters it and then sends it to the laser PZT

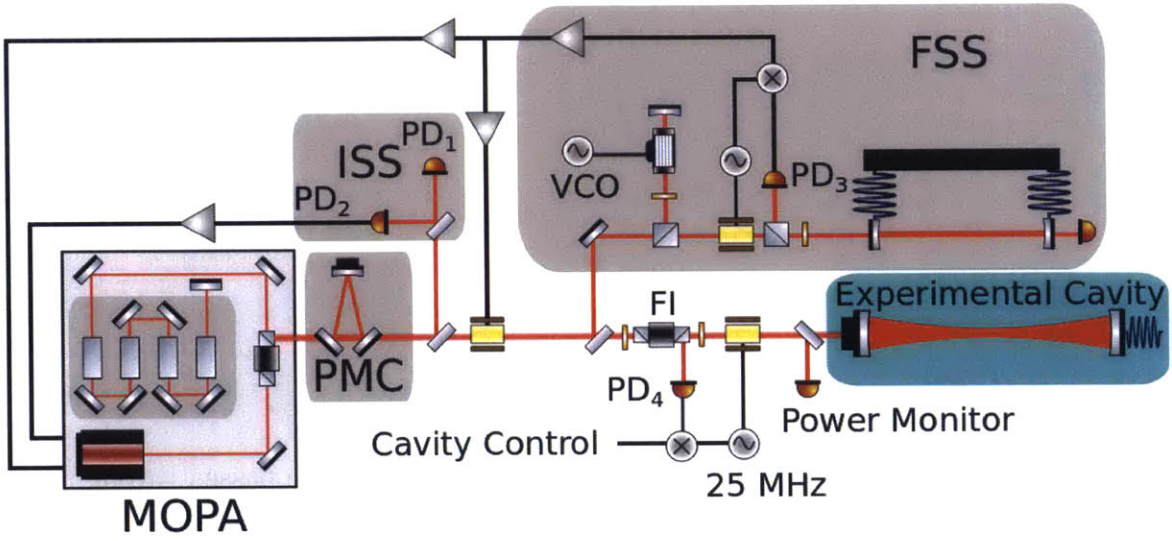

Figure 3-2: Schematic of the PSL. The laser passes through the pre-mode cleaner (PMC). Then a fraction of the light is split to perform intensity stabilization to the 10^{-8} level using PD2. PD1 provides and out of loop reference for the intensity noise. After the ISS a small amount of light is picked off and send to a suspended reference cavity which provides frequency stabilization. The majority of the light continues downstream through an electro-optic phase modulator (EOM) where 25 MHz RF sidebands are added for Pound-Drever-Hall (PDH) locking of the experimental cavity. The laser then passes through a Faraday isolator (FI) to protect the laser-cavity system from back reflections. A small amount of light is picked off to provide a reference for the amount of power entering the vacuum system.

and a broadband EOM in front of the laser. Changing the frequency of the VCO will shift the setpoint of the FSS servo loop and allows for the FSS to track another length or frequency reference. Here it will track the experimental cavity's length above 300 Hz.

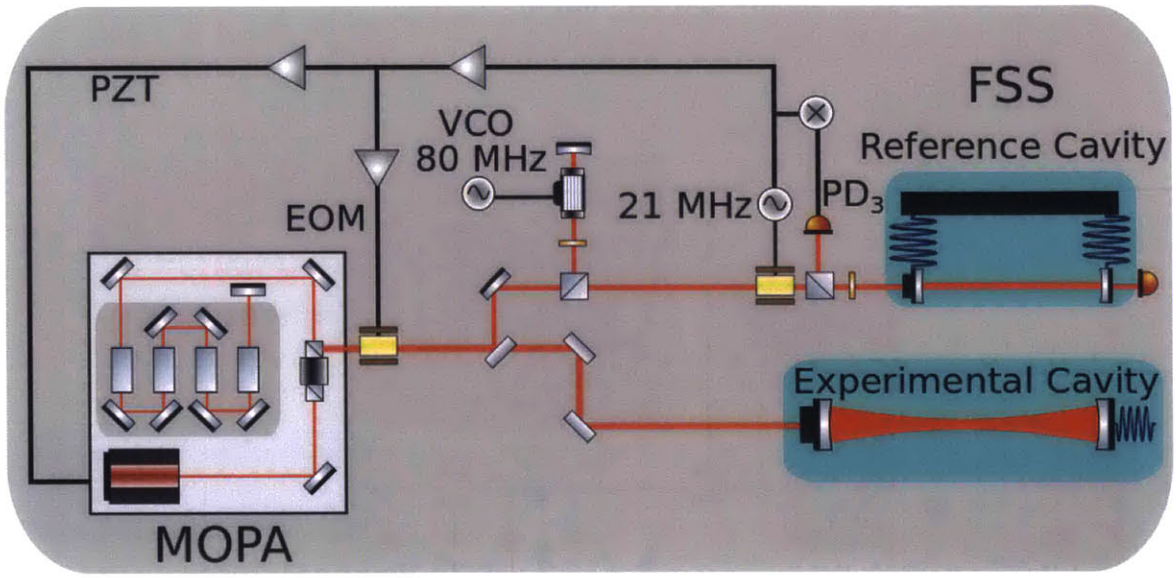

Figure 3-3: Schematic of the FSS. Light from the MOPA is double passed through an AOM that is driven by an approximately 80 MHz VCO resulting in a frequency offset from the main laser of 160 MHz. A resonant New Focus 4004 EOM provides 21 MHz phase modulation sidebands which are used to lock laser frequency of the MOPA to the reference cavity. This lock utilizes the laser PZT actuator at low frequencies and a broadband New Focus EOM before the FSS pickoff at high frequencies.

3.2 Experimental Cavity

Figure 3-4 shows the the cavity where the experiments are performed. In Table 3.1 is a list of the cavity parameters. Figure 3-5 shows a photograph of the cavity when the vacuum system was vented. The cavity is composed of two high reflectivity mirrors 1 meter apart. The input mirror is referred to as the input test mass (ITM) and is a 76.2 mm diameter, 25.4 mm thick optic with a mass of 250 grams. The end test mass (ETM) is an 12.7 mm diameter, 3 mm thick optic, with a mass of 1 gram. The power transmissions of the optics are 3 ppm and 800 ppm for the ETM and ITM, respectively. From other measurements of the reflected power drop when the cavity is

locked, we know that the cavity roundtrip loss not including the mirror transmissions is around 7 ppm. Using equation 2.31, this gives a cavity linewidth (FWHM), κ_{tot}, of around 19.323 kHz.

The experiment is setup as a Fabry-Perot Michelson interferometer, but for the purposes of the OMIT measurements will will only use one arm of the interferometer, and so we will omit information on the Michelson portion and the other arm.

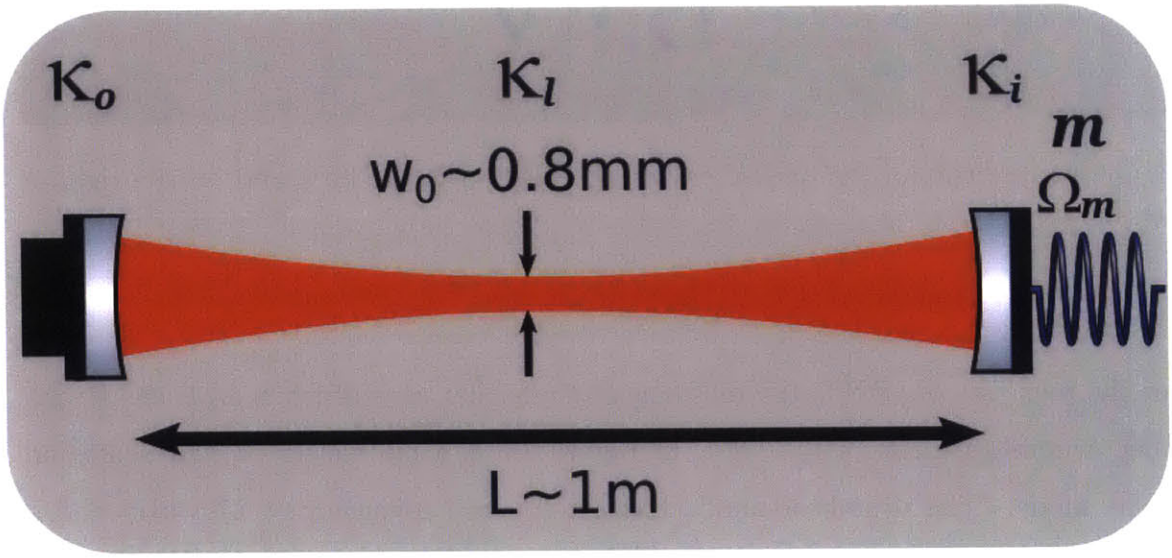

Figure 3-4: Schematic of the optical cavity. The length is 1 meter, with the beam waist in the middle, and the beam diameter at the optic surface being 1 mm. The ITM transmission is $\frac{\kappa_i}{2\pi}$ = 19.085 kHz. The ETM transmission is $\frac{\kappa_o}{2\pi}$ = 71.5 Hz. The cavity losses are $\frac{\kappa_l}{2\pi}$ = 166.0 Hz. The mechanical oscillator, which is the drumhead mode of the ITM has a modal mass (m) of approximately 150 grams and a resonance frequency ($\frac{\Omega_m}{2\pi}$) of 27.5 kHz.

Parameter	Symbol	Value
Output Loss Rate	κ_o	71.5 Hz
Input Loss Rate	$\frac{\kappa_i}{2\pi}$	19.085 kHz
Cavity Loss Rate	$\frac{\kappa_l}{2\pi}$	166.0 Hz
Length	L	1 m
Cavity Waist	w_0	0.8 mm

Table 3.1: Optical cavity parameters.

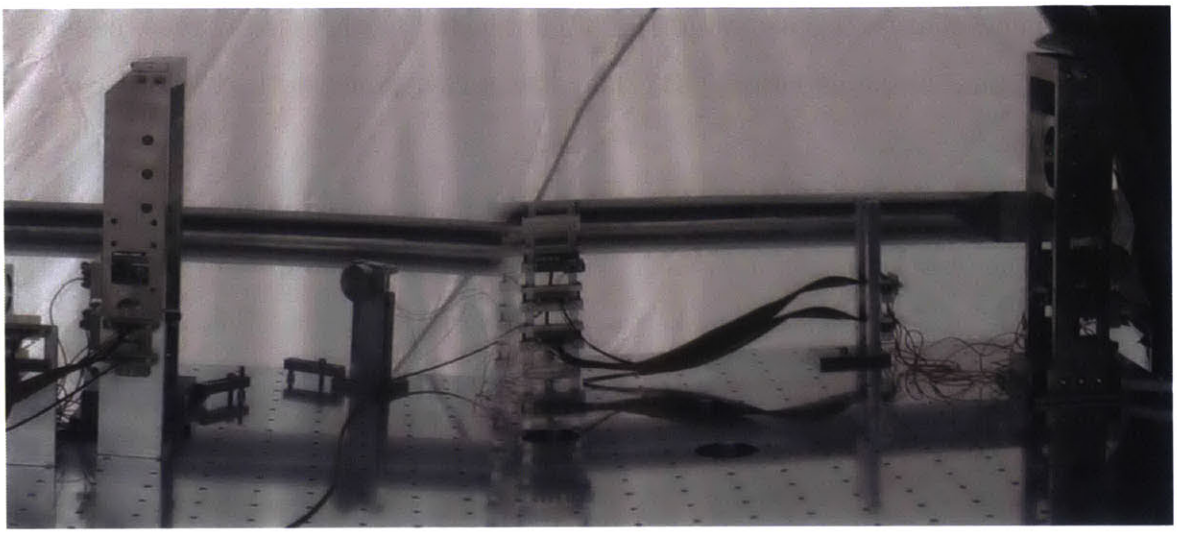

Figure 3-5: Picture of the optical cavity. On the left is the ITM and on the right is the ETM.

3.3 Mechanical Oscillator

For the purposes of OMIT, the mechanical mode that we will focus on is the lowest order drumhead mode of the ITM. In Figure 3-6 is a finite-element representation of the mode. The drumhead mode has a resonance frequency of 27.5 kHz and a reduced mass of 0.125 kg. The quality factor (Q) of the mode is around 10^6 giving a mechanical loss of $\frac{\Gamma_m}{2\pi} = 0.0275$ Hz.

Parameter	Symbol	Value
Resonance Frequency	$\frac{\Gamma_m}{2\pi}$	27.5 kHz
Modal Mass	m	125 grams
Quality Factor	Q	1.1×10^6

Table 3.2: Mechanical mode parameters.

3.4 Readout and Control

3.4.1 Readout

The experimental cavity has multiple readout systems. The first is a radio-frequency Pound-Drever-Hall (PDH) system operating at 25 MHz for locking the cavity on

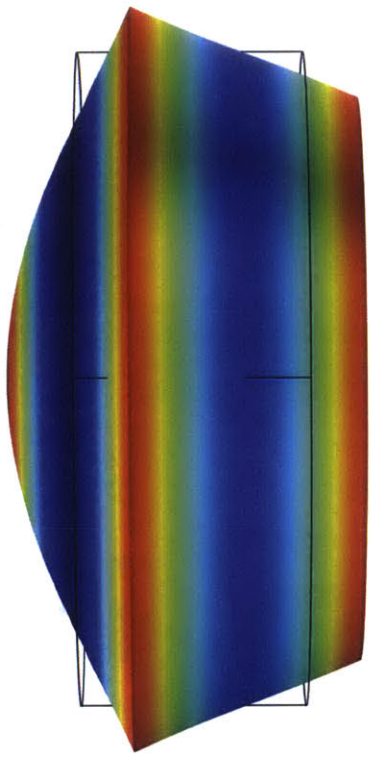

Figure 3-6: Finite element representation of the mechanical mode created with COMSOL. The wireframe show the unexcited optic.

resonance [3]. The second readout utilizes the light transmitted through the cavity to perform a DC lock on the side of the fringe. Figure 3-7 shows the two readout systems and their regimes of operation.

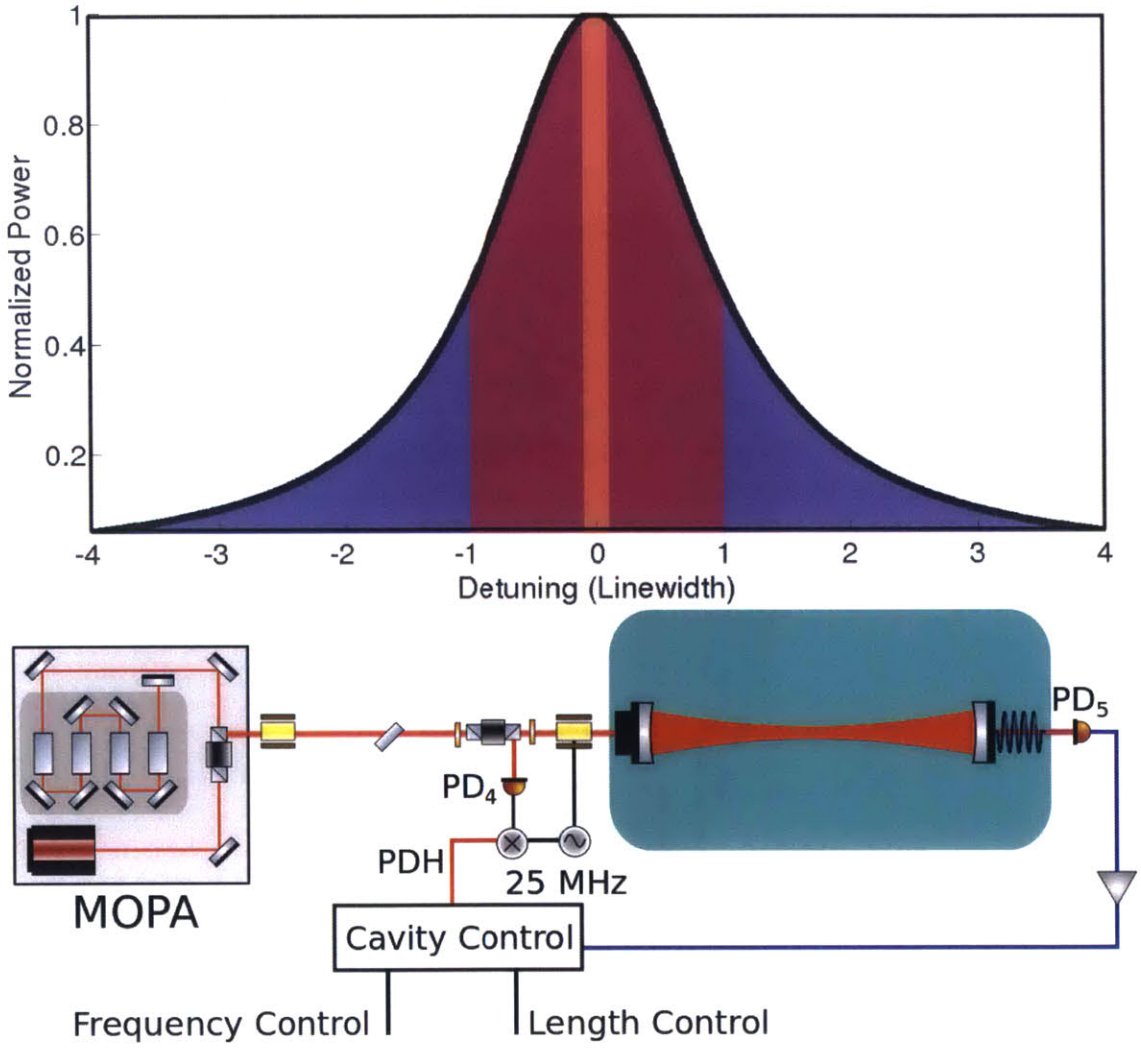

Figure 3-7: Schematic of the two readout systems and their respective regimes of operation. The Pound-Drever-Hall (PDH) readout is operated in reflection and is indicated by the red shading on the cavity power transmission curve. The PDH readout can be used from about -1 to 1 linewidth detuning. It is designed to operate at zero detuning. The transmitted light readout uses a side of fringe readout and is valid for non-zero detunings. In practice the operational regime is limited by the sensitivity of the photodetector and the residual cavity motion. Here we have added an arbitrary stop at 0.1 linewidth. The transmitted light readout is indicated by the blue shading on the power transmission curve.

Pound-Drever-Hall readout

The PDH locking signal is generated with a 25 MHz sideband impressed on the main beam via an EOM. The error signal is generated via the reflected light using a LIGO resonant RF photodiode (D980454-D), denoted as PD_4 in Figure 3-7. It is then demodulated via a LIGO demod board (D990511). The signal is then split, part goes into a computer system where it is digitally filtered and then fed back to coil-magnet actuators (OSEM) on the cavity optics [9, 31]. This changes the length of the cavity. A second part of the signal is routed throught the Common Mode Board (D040180 Rev B) where it is fed to the VCO which changes the laser frequency by pulling the FSS lock point.

Transmitted Light Readout

To lock detuned, we use a side of fringe lock utilizing the slope of the transmitted light. For this signal, we detect the light tranmitted through the cavity on a photodiode (PD_5). This signal is then fed to both the digital system and the common mode board where it is then fed back to the cavity length and the frequency of the laser, respectively.

3.4.2 The Control System

Cavity Control

The control of the cavity length is performed via a digital-analog hybrid with two different actuation paths. At low frequencies, below 300 Hz, the readout is fed into a digital system where is it processed and then routed to the coil-magnet actuators on the ITM. This actuates the cavity length. At higher frequencies the cavity control is performed by changing the laser frequency via the VCO control point of the FSS loop. A simplified version of this is shown in Figure 3-8.

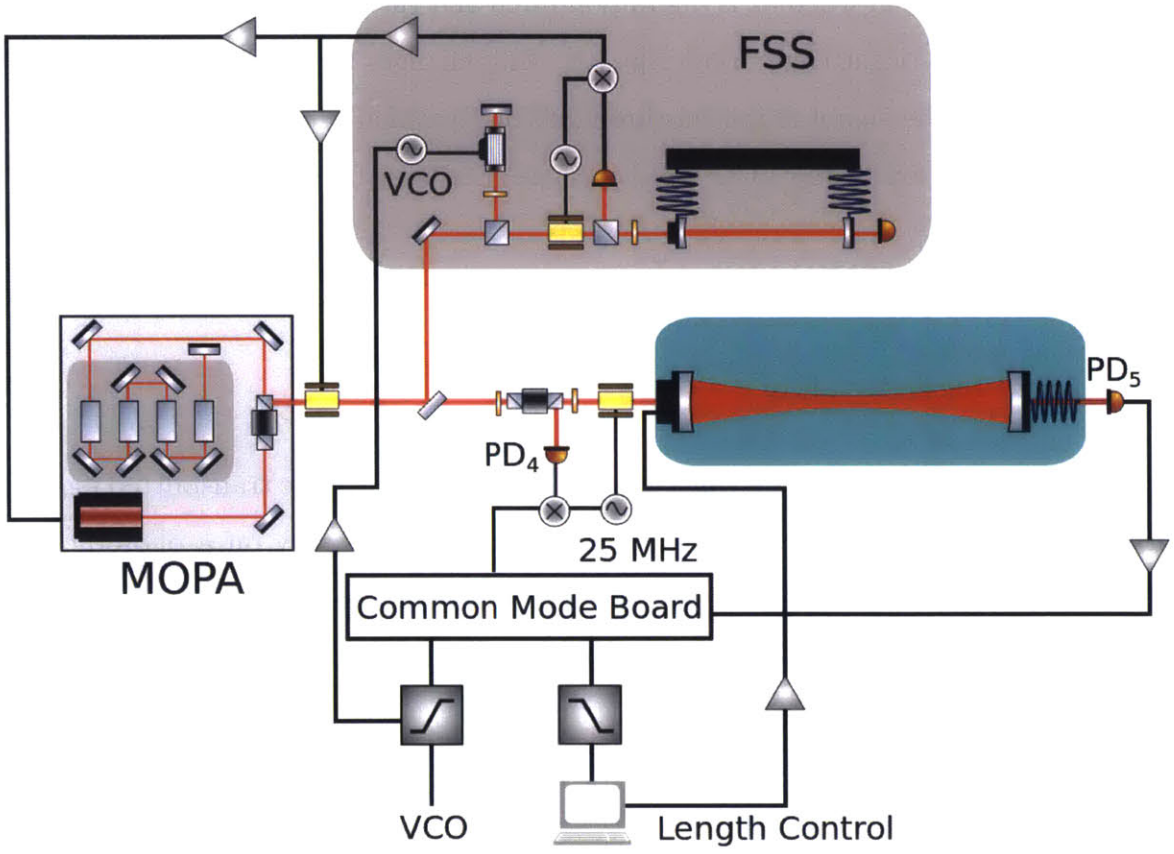

Figure 3-8: Diagram of the cavity control. At low frequencies, below 300 Hz, the cavity is controlled via actuation directly to the optics. At high frequencies, above 300 Hz and below 1100 Hz, the cavity is controlled by changing the frequency of the laser.

Control Handoffs

In some situations, it is easier to lock the cavity either detuned (TRANS) or on resonance (PDH), but the desired operation point is in the opposite regime. To transition between these regimes, we handoff the cavity control from one control signal to the other. To do this we must be in a regime where both signal provide valid length information about the cavity length. For example, we can not hand off the controls on resonance, since the TRANS signal vanishes, or above 1 linewidth detuning, the PDH signal vanishes.

Assuming that the filters in each signal path are set correctly, for example they are both whitened to the same level, then handing off involves turning one signal's gain down while ramping the other up. To hand off from Signal A to B, we first find the desired gain value for Signal B. To do this, we perform a single point FFT of the two control signals at their crossover frequency. We then obtain the desired gain G_b from $\frac{A(f)}{B(f)}$. Once we have obtained the desired gain G_b we can then ramp the gain of Signal B up while simultaneously ramping Signal A's gain down. This process is automated via scripts, most specifically /data/pde/scripts/red_handoff.py. In addition, to the red_handoff script, automatic servos control the unity gain frequency and crossover of the CARM length path servo. These are referred to as the ugf servo. The ugf servo, takes a signal point transfer function to measure the crossover and unity gain frequency which is then used to correct the gain of the CARM and frequency path loops. The crossover frequency is commonly set to 300 Hz and the unity gain around 10 kHz for a single arm lock.

Chapter 4

Measurement of extreme optomechanically induced transparency

In this chapter we will present a measurement of OMIT that has a linewidth (FWHM) of almost 10 mHz.

4.1 Locking Procedure

As mentioned previously in the Chapter 2, to create the conditions for OMIT, the cavity needs to be locked with reddetuning at the mechanical resonance frequency. In other words, when the mechanical mode has a frequency of Ω_m, we want to set the cavity detuning for the pump field at $\delta = -\Omega_m$. Since we are locking outside of the cavity linewidth a PDH signal gives no useful information. Therefore the lock during the measurement needs to be performed using the transmitted light.

Acquiring lock red-detuned is significantly more difficult that acquiring either blue-detuned or on resonance due to the fact that there is a strong optical anti-spring. This anti-spring makes the cavity much more susceptible to any external disturbances such as seismic fluctuations and makes achieving the lock more difficult. To alleviate this problem the locking procedure is as follows:

1. Lock the cavity on resonance at 120 mW using the PDH error signal.

2. Turn off the frequency path ugf servo since we will be detuning the cavity and this will mess up the servo.

3. Red detune the cavity to approximately 90% of the power on resonance. In practice, since the common mode board (CMB) has an offset depending on the gain, by lowering the gain of the demod path by 10 dB and raising the VCO gain to 30, this will naturally put the cavity at around 90% of the undetuned power.

4. Turn off the triggers and suspend the autorun script.

5. Since the triggers and the autorun script provide much of the safety when the lock breaks we use a script called watch_trans.py to make sure that we don't blow out any photodiodes. Run the script watch_trans.py

6. Hand off the length path from REFL(PDH signal), to TRANS (side of fringe signal). Note, this now is setting the detuning, not the CMB.

7. Hand off the frequency path.

    - Turn the gain in the trans path all the way down to -32 dB.
    - Run the script slow_cav that takes care of any offset problems.
    - Turn up the trans path gain slowly until the CARM ugf servo has increased the length gain by a factor of 2. When this happens it indicates that the trans path gain is equal to the demod path gain (at the crossover point).
    - Ramp off the demod path gain. The ugf servo will set the gains automatically.

8. The handoff is complete, the next step is to ramp the trans_offset to the value that corresponds to the correct detuning.

This procedure procedure is summarized schematically in Figure 4-1.

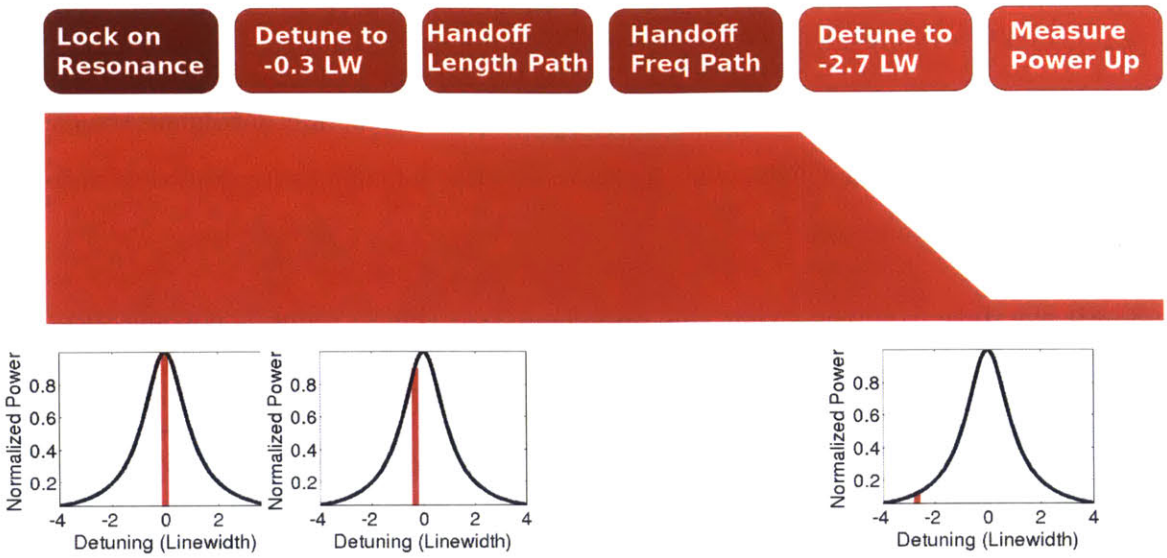

Figure 4-1: A schematic of the locking sequence

4.2 Measurement Procedure

To measure OMIT, we need the basic setup of strong coupling between a mechanical oscillator and a cavity that is red-detuned. The optimal detuning is the mechanical resonance frequency. Beyond the mechanical oscillator, the cavity, and the pump laser, a probe laser is needed to measure the modification of the optical transfer function due to the optomechanical coupling. Since we don't have a second laser that can be used as the probe field, we take advantage of the fact that we are far detuned from the resonance (approxmiately 2.7 linewidths). Therefore we can use a frequency (phase) modulation excitation to approximate the effect of a single probe laser. The reason for this is that if we are detuned by an amount δ from the resonance, we need to put on a frequency excitation that is also of order δ. If we are red-detuned, then the upper sideband from the modulation will be at zero detuning, and the lower sideband will be at 2δ which in this case is far outside the cavity linewidth. The effect of the lower sideband is taken into account in the fitting procedure. See Figure 2-2 for frequency space plot of the fields involved.

The measurement procedure is as follows:

1. Lock the cavity red-detuned and set the detuning to the mechanical linewidth,

as detailed in Section 4.1.

2. Using a SR785 network analyzer to perform a swept sine measurement, exciting at the output of the CMB, from 5 kHz to 60 kHz. This measurement determines the cavity parameters.

3. Fit the data from the swept sine and check that the detuning is correct. If not, correct the detuning and repeat.

4. After the detuning has been verified, perform a swept sine through the CMB that is right around the resonance.

5. Ramp the cavity power up, let the cavity heat stabilize due to absorption, repeat the previous step.

4.3 Correcting and Fitting the Data

The measurement procedure above gives us plots that look like the OMIT feature but need to be corrected for a variety of reasons.

- Intracavity power depends on cavity mirror alignment.
- Frequency excitation is in-loop.
- Frequency dependence of the transmitted PD.
- Readout is in-loop.
- Excitation is in frequency and not phase.

The first item in the list is the easiest to correct for. At low power we assume that we are aligned. When we lock the cavity we know that in the undetuned state we have N counts on the transmitted photodiode at input power P_0. When we detune offset Δ, we have $N_{det} = \frac{N}{1+\Delta^2}$ counts on the transmitted photodetector. When we power up from P_0 to αP_0 the number of counts should scale linearly, assuming that the PD

response is linear so we can reset the TRANS offset to get the correct detuning. If we measure the detuning and it is not what we think it should be then we attribute the discrepancy to that fact that DC radiation pressure has caused misalignments in the cavity axis. We correct for that using the following steps:

1. At low power we assume that we are aligned. We set the detuning to -Ω_m at P_0. Call the transmitted counts T_0.

2. Power up to $P_1 = \alpha P_0$. Set the transmitted counts to $T_1 = \alpha T_0$.

3. Take a wideband transfer function and fit the data, this provides a measure of the detuning. If it is not equal to the detuning for T_0 then the alignment is off and the actual power is. This then allows you to correct the detuning for the new power level using the $P_{new} = \alpha P_o \frac{1+\delta_1^2}{1+\delta_0^2}$

After correcting for misalignments, and before fitting, we need to correct the data for the other loop effects mentioned above. The easiest way to see how to do this is to look at a loop diagram of the measurement, shown in Figure 4-2.

From the loop diagram we can get a more complete picture of how to disentangle the information that we need from the measurement. What we measure on the SR785 is $\frac{V_1}{V_2}$. Going around the loop diagram we find for V_1:

$$(V_1 \cdot F_{CMB} + V_{exc}) \cdot F_{freq} \cdot F_{act} \cdot t_{OMIT} \cdot F_{PD} \cdot F_{FB} \cdot F_{560} = V_1 \tag{4.1}$$

$$V_1(1 - \underbrace{F_{CMB} \cdot F_{freq} \cdot F_{act} \cdot t_{OMIT} \cdot F_{PD} \cdot F_{FB} \cdot F_{560}}_{G_{freq}}) \tag{4.2}$$

$$= V_{exc} \cdot F_{freq} \cdot F_{act} \cdot t_{OMIT} \cdot F_{PD} \cdot F_{FB} \cdot F_{560}$$

$$V_1 = V_{exc} \frac{G_{freq}}{1 - G_{freq}} \frac{1}{F_{CMB}} \tag{4.3}$$

and for V_2:

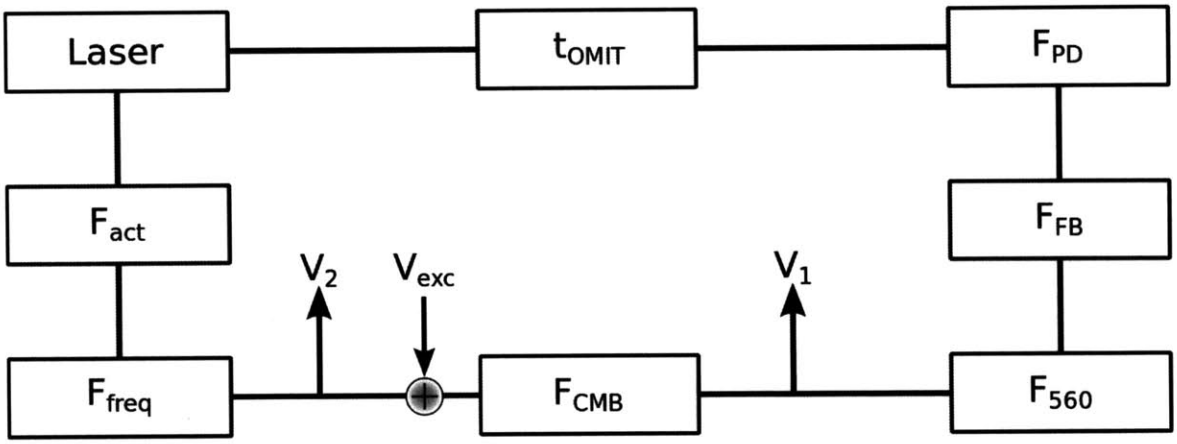

Figure 4-2: Loop diagram of the OMIT measurement. We are measuring $\frac{V_1}{V_2}$. We excite the CMB which causes the a modulation on the frequency of the laser via the FSS loop, denoted as F_{act}. This modulation then enters the cavity and interacts with the mechanical element via radiation pressure. The optomechanical transfer function is denoted as t_{OMIT}. The light transmitted through the cavity is detected on a photodiode. The photodiode responce as a function of frequency is F_{PD}. The signal from the PD is then passed through an analog filter board F_{FB}, and a SR560, F_{560}. Part of the signal is picked off at this point, V_1, and sent to a SR785 to be used for the swept sine transfer function measurement. In addition, the signal travels through the CMB, F_{CMB}. After the CMB we then sum in the excitation and pick off a second measurement point, V_2 that is also sent to the SR785.

$$\begin{aligned} V_2 &= V_2 \cdot F_{freq} \cdot F_{act} \cdot t_{OMIT} \cdot F_{PD} \cdot F_{FB} \cdot F_{560} \cdot F_{CMB} + V_{exc} \\ &= V_{exc} \frac{1}{1 - G_{freq}} \end{aligned} \tag{4.4}$$

Then combining equations 4.3 and 4.4 we get:

$$\frac{V_1}{V_2} = \frac{G_{freq}}{F_{CMB}} \tag{4.5}$$

or for our purposes:

$$t_{OMIT} = \frac{\frac{V_1}{V_2}}{F_{freq} \cdot F_{act} \cdot F_{PD} \cdot F_{FB} \cdot F_{560}} \tag{4.6}$$

All that remains to correct the measured transfer functions is to measure F_{freq}, F_{act}, F_{PD}, F_{FB}, and F_{560}. F_{act} is the only non-trivial transfer function to measure since in the model above we are asking what is frequency excitation that comes from exciting the CMB. This frequency excitation utilizes the FSS loop to actuate on the frequency of the laser. So F_{act} is actually the closed loop transfer function of the FSS loop. See Figure 4-3 for more details.

In Figures 4-4, 4-6, 4-5, and 4-7 are the measured transfer functions used to perform the corrections.

4.4 Fitting the Data

After the data has been corrected, we then take the model from Chapter 2 and fit it to the data. For each pump power level we have two sets of data. The first set is a wideband, 5 kHz to 60 kHz, transfer function that does not show the OMIT feature, since the feature is so narrow. The second set is a narrowband transfer function localized around the mechanical mode frequency that shows the OMIT feature. The parameters that we would like to fit with our model include the following:

- Modal mass , m

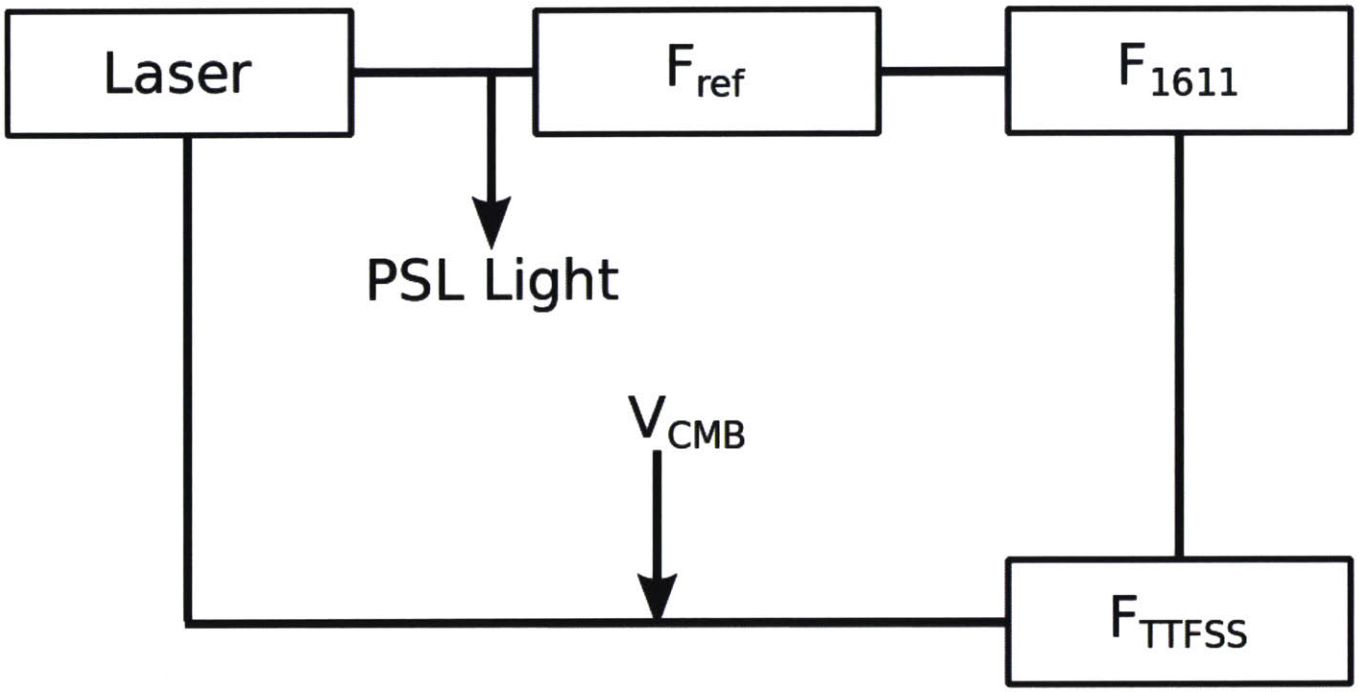

Figure 4-3: Simplifed FSS loop. F_{ref} is the optical transfer function of the reference cavity, f_{1611} is the transfer function of New Focus 1611 photodiode used to measure the PDH error signal for the reference cavity, and F_{TTFSS} is the transfer function of the filter and actuation used to lock the FSS.

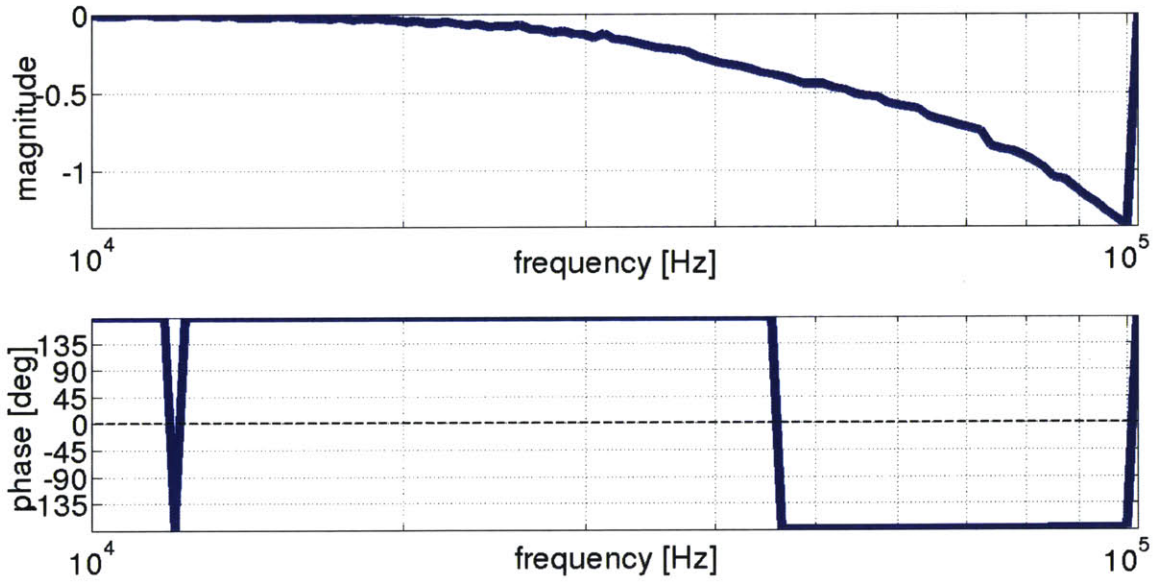

Figure 4-4: Bode plot of F_{act} or the closed loop gain of the FSS loop, $\frac{G_{FSS}}{1-G_{FSS}}$.

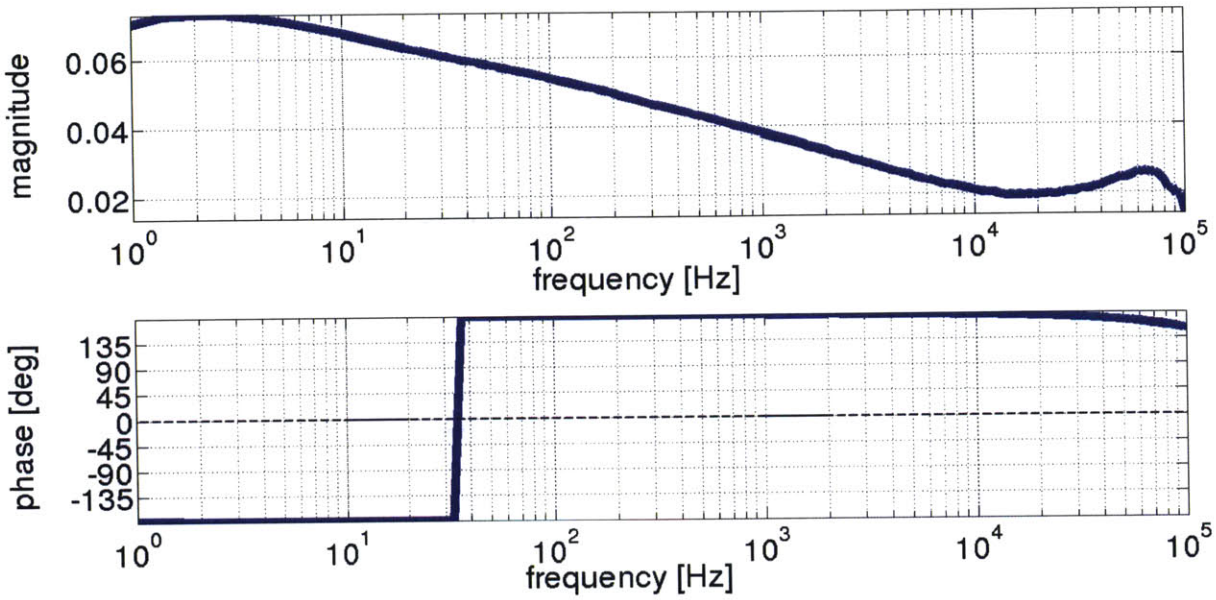

Figure 4-5: Bode plot of the tranfer function, F_{560}, of the SR560 in the feedback path

.

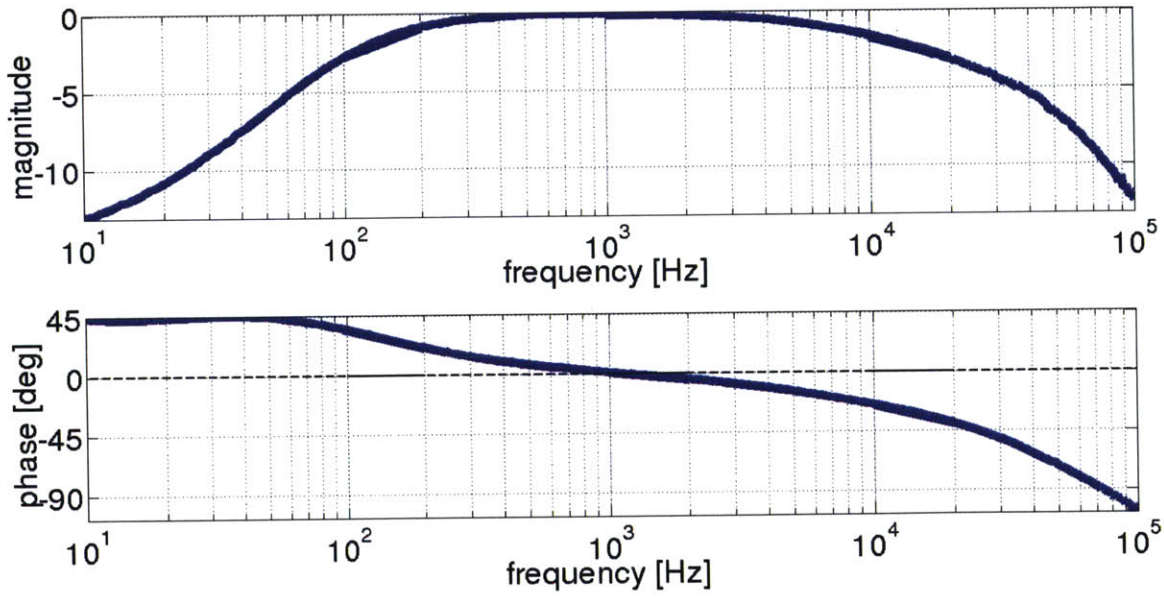

Figure 4-6: Transfer function of the transmitted light photodiode, F_{PD}.

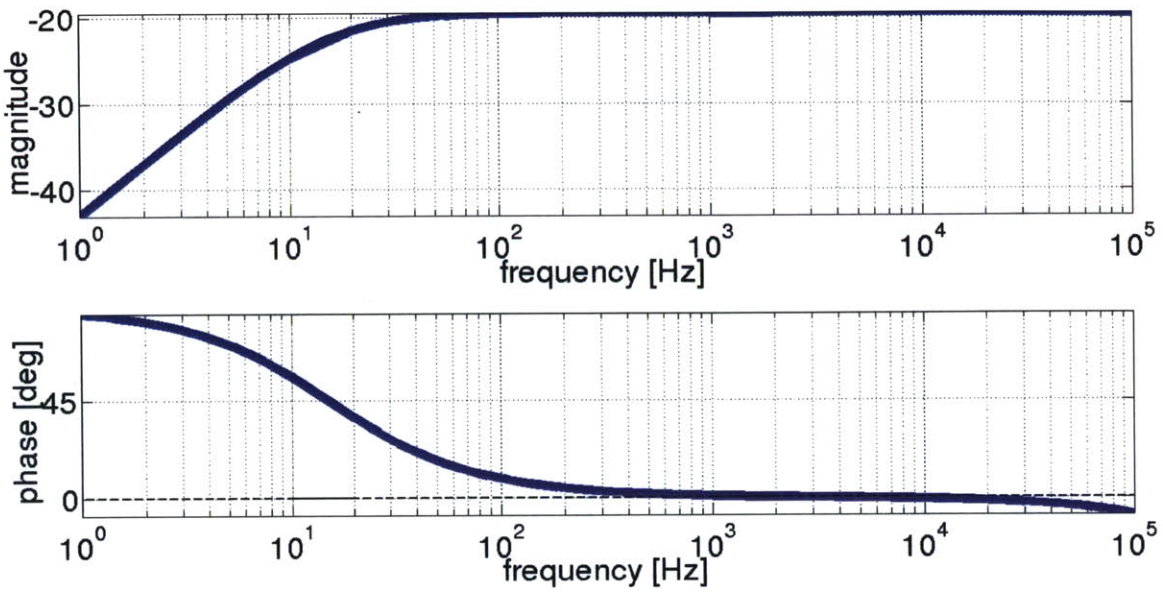

Figure 4-7: Transfer function of the cavity feedback filter board, F_{FB}.

- Mechanical resonance frequency, Ω_m
- Mechanical mode damping, Γ_m
- Pump power, P
- Detuning, Δ
- Total cavity loss, or FWHM of the cavity, κ_{tot}

Because we are detuned, the asymmetric sideband response of the cavity gives information about both, Δ and κ_{tot}. The narrowband transfer functions will give information about m, Ω_m, and Γ_m. The fitting procedure is as follows:

1. Fit the wideband transfer functions at power P_i for Δ and κ_{tot}.
2. Using the values of Δ and κ_{tot} from the wideband fit, we fit the narrowband transfer function for m, Ω_m, Γ_m. The fitting routine fits for all parameters, but both κ_{tot} and Δ are restricted to be within one percent of values from the wideband transfer function.

In Figures 4-8, and 4-9 we show plots of a representative wideband and narrowband fit along with the fit residuals. As seen in the plots, the data is fit extremely well. Figure 4-10 is a plot of the OMIT feature as a function of power. In this plot, we see how the OMIT dip increases as a function of power and the OMIT linewidth also increases. Also apparent from the figure, the dip gets deeper and wider as the power is increased. This can be seen in more detail in Figure 4-12 where the linewidth of the dip is plotted as a function of power. Extracting the cooperativity from all of the different power levels gives the plot in Figure 4-11. The fitted value of 0.035 agrees quite well with the predicted value of 0.031 $\pm$ 0.005 calculatd using the fit parameters. Figure 4-13 which shows how the different fit parameters varied as a function of power. We extract a value of $\frac{\kappa_{tot}}{2*2\pi}$ of 10.7 kHz $\pm$ 0.18 kHz. The reduced mass of the oscillator is 133 grams $\pm$ 9.6 grams. The mechanical loss, $\frac{\Gamma_m}{2\pi}$, is 23.8 mHz $\pm$ 3.2 mHz, corresponding to a quality factor of 1.2×10^6. This is approximately what is to be expected from fused silica.

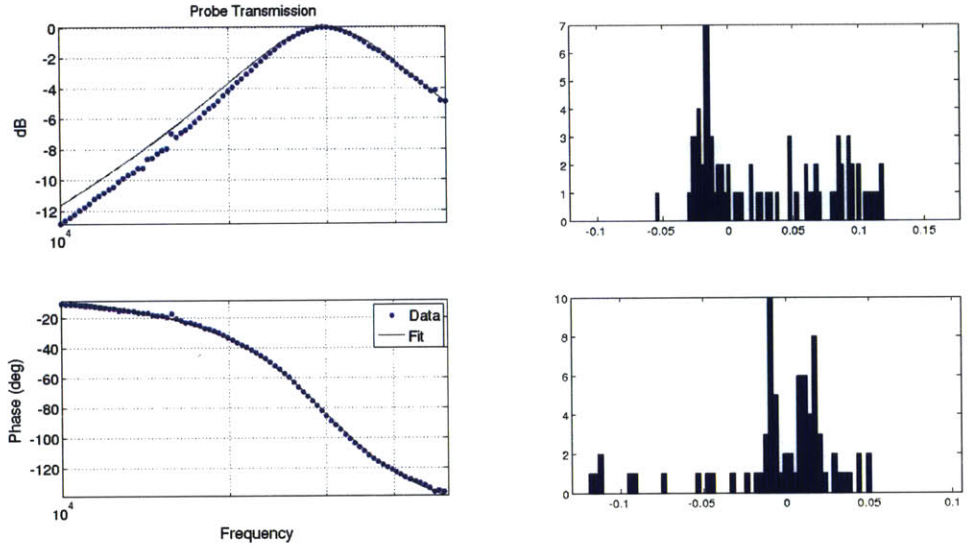

Figure 4-8: A sample wideband fit. Here the input power was 61 mW.

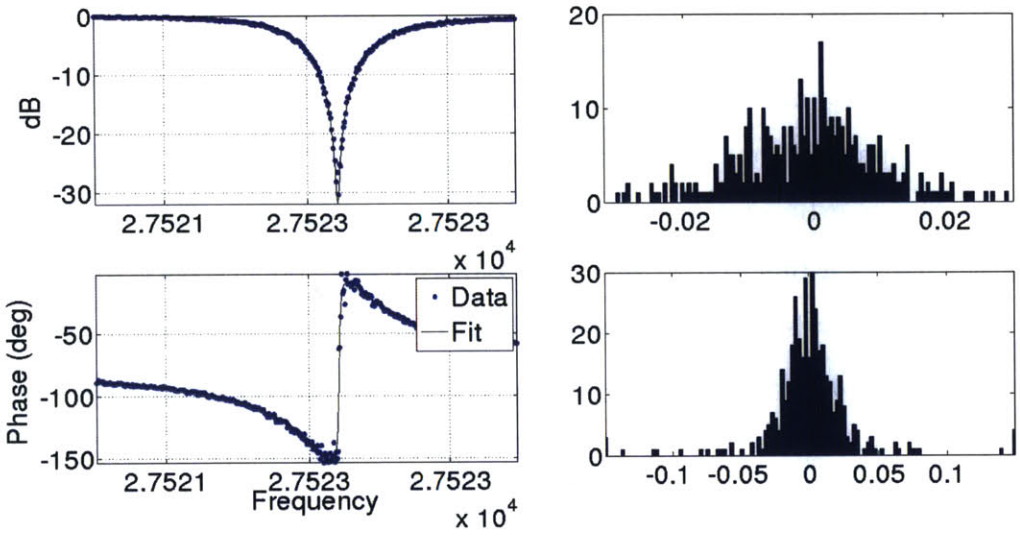

Figure 4-9: A sample narrowband fit. Here the input power was 1180 mW.

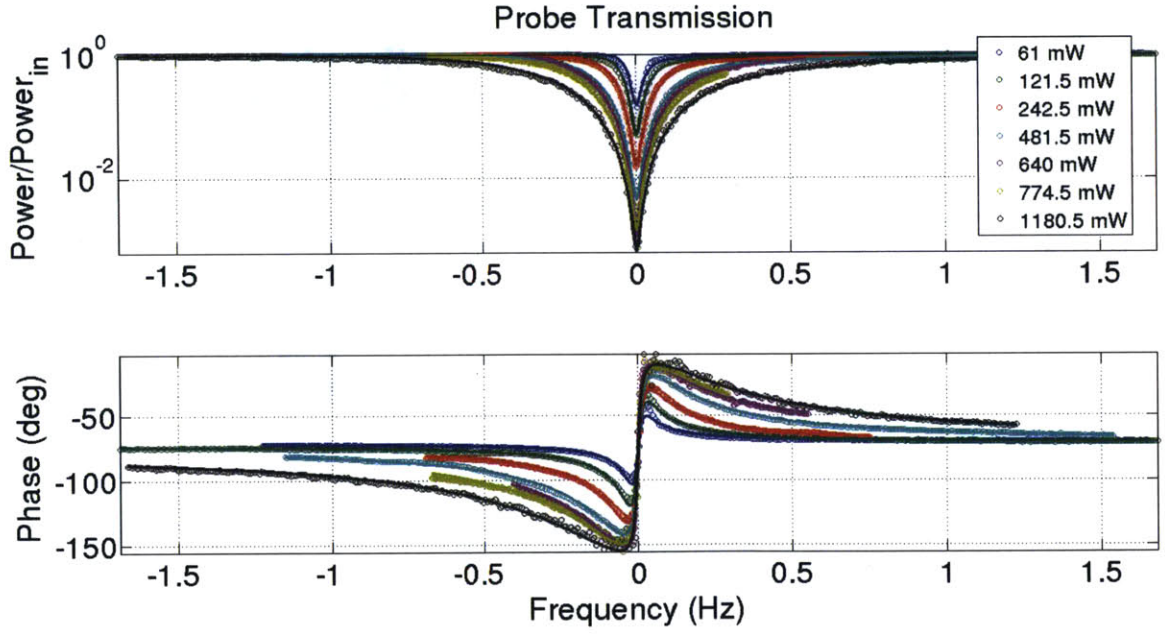

Figure 4-10: A plot of the OMIT dip as a function of power.

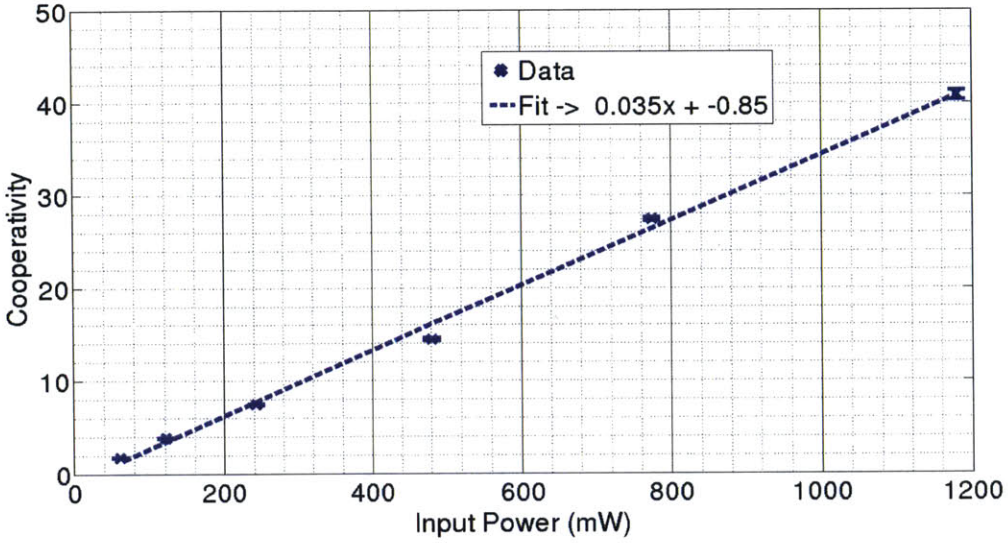

Figure 4-11: A plot of the cooperativity as a function of the power. As you can see this is very well fit by a linear curve with a slope of 0.035. This compares very well to a calculated value of 0.031 $\pm$ 0.005 obtained from the average fitted values of m, Δ, κ_{tot}, and Γ_m.

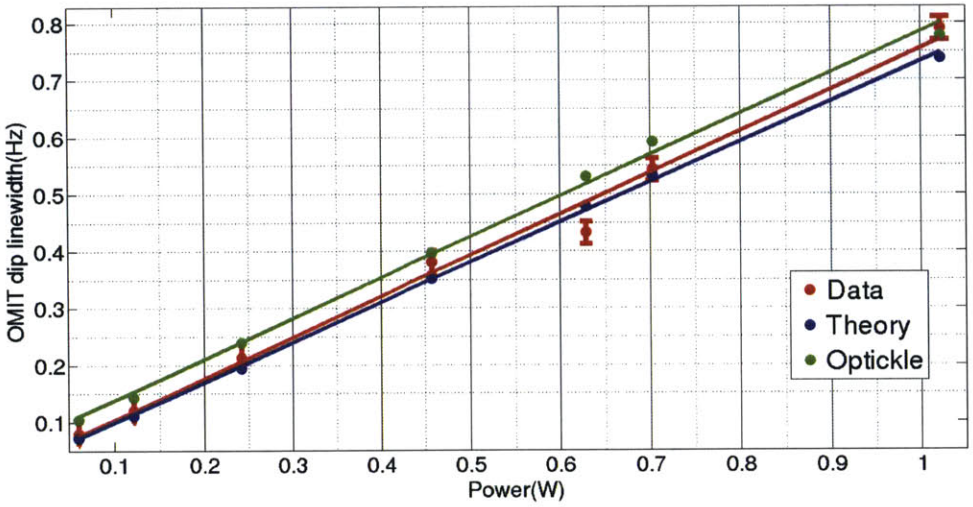

Figure 4-12: A plot of the linewidth of the OMIT feature as a function of laser power found in three different ways. The red line has a slope of 0.7239 and the linewidth is extracted from the measured data. The blue line has a slope of 0.7041 and is calculated using the fit parameters in a theoretical model. Finally, the green curve is calculated using the fit parameters and inputting them into Optickle, an interferomter modelling program. Optickle generates OMIT curves and then the linewidth is measured from those curves. As shown from the plot, the data is linear as a function of power which is what we expect and follows very closely to the predicted slope give by the blue line.

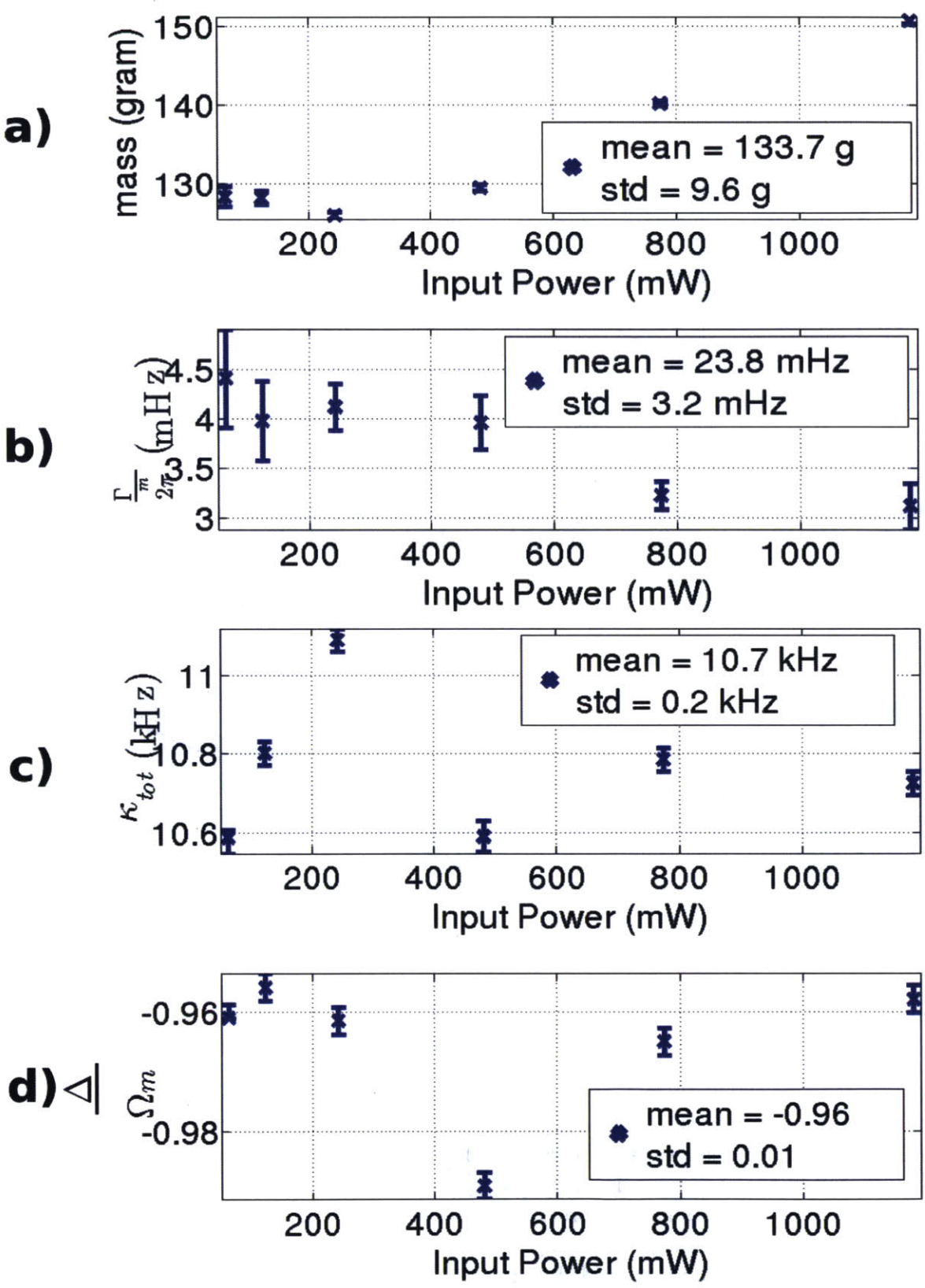

Figure 4-13: Plots of the fit parameters for **a)** modal mass m, **b)** $\frac{\Gamma_m}{2\pi}$, **c)** $\frac{\kappa_{tot}}{2\pi}$ and **d)** Δ as a function of the power.

Chapter 5

Future Directions

In the previous chapters, we have described the theory behind OMIT, along with an experimental setup that has measured the smallest OMIT linewidth known to us. OMIT has a wide variety of applications, but many are dependent on the width of the OMIT feature since this provides a timescale.

At larger OMIT linewidths (on the order of 10 to 100 Hz), OMIT offers the possibility of creating a tunable filter cavity for quantum noise. This has many applications for gravitational wave detection and there has been a theoretical study done in [17]. In addition, the base linewidth of the OMIT filter cavity should be less than the minimum required for the system. In this sense, our system with its extremely narrow linewidth is ideal. On the other hand, at some point the intensity noise of the control laser will become an issue for quantum mechanical applications, so the system needs to be designed to minimize this effect.

For a system to work as a quantum noise filter, there are much more stringent requirements on both the pump laser and the mechanical system. Usually, for a gravitational wave detector filter cavity, the relevant quantity is the optical loss per length. This is due to the fact that a filter cavity uses the optical linewidth to rotate the quadrature of the input quantum noise. This linewidth can be changed via changing the length or changing the loss per roundtrip in the cavity. To use OMIT in place of an optical cavity in this situation requires that the mechanical system be in the quantum ground state. The physical reason for this can be seen by looking at the

OMIT level diagram in relation to a standard optical cavity. Looking at the OMIT level diagram shows that linewidth of the OMIT cavity is defined by the intrinsic mechanical loss and broadening due to saturation of the OMIT dip.

From this perspective, to use OMIT for a filter cavity in gravitational wave detection, the mechanical linewidth needs to lower than the linewidth of the arm cavities. This way the cavity can be tuned through the linewidth of the arm cavity while still operating in a saturated regime.

To put some numbers on this, the Advanced LIGO arm cavity pole is at around 40 Hz, so the mechanical oscillator would possibly have a linewidth of around 40 Hz. Since this value is very high it could be artificially changed by replacing the mechanical oscillator with another optomechanical system where the frequency of the optomechanical oscillator are defined via an optical spring and optical damping.

Another possible way to use OMIT with small mechanical linewidths is to use the OMIT dip as a reference to lock two lasers together, similar to frequency stabilization. In this case the linewidth would be as small as possible, neglecting other noise sources. Using the OMIT dip as a reference has one crucial difference as compared to a fixed reference cavity: the OMIT dip uses a pump laser to mediate the interaction. This means that any frequency shift of the pump laser will change the relative width of the OMIT dip. Therefore, OMIT will allow for locking two lasers relative to each other very tightly as defined by the mechanical linewidth, but not absolute frequency stabilization.

Bibliography

[1] G. S. Agarwal and S. Huang. Electromagnetically induced transparency in mechanical effects of light. *Physical Review A*, 81(4):041803, April 2010.

[2] T. Baba. Slow light in photonic crystals. *Nature Photonics*, 2:465–473, 08 2008.

[3] Eric D. Black. An introduction to pound drever hall laser frequency stabilization. *American Journal of Physics*, 69(1):79–87, 2001.

[4] K.-J. Boller, A. Imamolu, and S. E. Harris. Observation of electromagnetically induced transparency. *Phys. Rev. Lett.*, 66:2593–2596, May 1991.

[5] Alessandra Buonanno and Yanbei Chen. Signal recycled laser-interferometer gravitational-wave detectors as optical springs. *Phys. Rev. D*, 65:042001, Jan 2002.

[6] J. Chan, T. P. M. Alegre, A. H. Safavi-Naeini, J. T. Hill, A. Krause, S. Gröblacher, M. Aspelmeyer, and O. Painter. Laser cooling of a nanomechanical oscillator into its quantum ground state. *Nature*, 478:89–92, October 2011.

[7] Y. Chen. Macroscopic quantum mechanics: theory and experimental concepts of optomechanics. *Journal of Physics B Atomic Molecular Physics*, 46(10):104001, May 2013.

[8] LIGO Scientific Collaboration. Observation of a kilogram-scale oscillator near its quantum ground state. *New Journal of Physics*, 11(7):073032, 2009.

[9] Thomas Corbitt. *Quantum Noise and Radiation Pressure Effects in High Power Optical Interferometers.* PhD thesis, MIT, 2008.

[10] Thomas Corbitt, Yanbei Chen, Edith Innerhofer, Helge Müller-Ebhardt, David Ottaway, Henning Rehbein, Daniel Sigg, Stanley Whitcomb, Christopher Wipf, and Nergis Mavalvala. An all-optical trap for a gram-scale mirror. *Phys. Rev. Lett.*, 98:150802, Apr 2007.

[11] Thomas Corbitt, David Ottaway, Edith Innerhofer, Jason Pelc, and Nergis Mavalvala. Measurement of radiation-pressure-induced optomechanical dynamics in a suspended fabry-perot cavity. *Phys. Rev. A*, 74:021802, Aug 2006.

[12] M. Eichenfield, J. Chan, R. M. Camacho, K. J. Vahala, and O. Painter. Optomechanical crystals. *Nature*, 462:78–82, November 2009.

[13] Michael Fleischhauer, Atac Imamoglu, and Jonathan P. Marangos. Electromagnetically induced transparency: Optics in coherent media. *Rev. Mod. Phys.*, 77:633–673, Jul 2005.

[14] S. Gigan, H. R. Böhm, M. Paternostro, F. Blaser, G. Langer, J. B. Hertzberg, K. C. Schwab, D. Bäuerle, M. Aspelmeyer, and A. Zeilinger. Self-cooling of a micromirror by radiation pressure. *Nature*, 444:67–70, November 2006.

[15] T. J. Kippenberg, S. M. Spillane, and K. J. Vahala. Demonstration of ultra-high-q small mode volume toroid microcavities on a chip. *Applied Physics Letters*, 85(25):6113–6115, 2004.

[16] Mikhail D. Lukin, Michael Fleischhauer, Marlan O. Scully, and Vladimir L. Velichansky. Intracavity electromagnetically induced transparency. *Opt. Lett.*, 23(4):295–297, Feb 1998.

[17] Yiqiu Ma, Stefan L. Danilishin, Chunnong Zhao, Haixing Miao, W. Zach Korth, Yanbei Chen, Robert L. Ward, and D. G. Blair. Narrowing the filter-cavity bandwidth in gravitational-wave detectors via optomechanical interaction. *Phys. Rev. Lett.*, 113:151102, Oct 2014.

[18] William Marshall, Christoph Simon, Roger Penrose, and Dik Bouwmeester. Towards quantum superpositions of a mirror. *Phys. Rev. Lett.*, 91:130401, Sep 2003.

[19] Osamu Miyakawa, Robert Ward, Rana Adhikari, Matthew Evans, Benjamin Abbott, Rolf Bork, Daniel Busby, Jay Heefner, Alexander Ivanov, Michael Smith, Robert Taylor, Stephen Vass, Alan Weinstein, Monica Varvella, Seiji Kawamura, Fumiko Kawazoe, Shihori Sakata, and Conor Mow-Lowry. Measurement of optical response of a detuned resonant sideband extraction gravitational wave detector. *Phys. Rev. D*, 74:022001, Jul 2006.

[20] A. F. Pace, M. J. Collett, and D. F. Walls. Quantum limits in interferometric detection of gravitational radiation. *Phys. Rev. A*, 47:3173–3189, Apr 1993.

[21] Jameson Rollins. Intensity stabilization of a solid-state laser for interferometric gravitational wave detectors. Master's thesis, MIT, 2004.

[22] Jameson Rollins, David Ottaway, Michael Zucker, Rainer Weiss, and Richard Abbott. Solid-state laser intensity stabilization at the 10< sup>-8</sup> level. *Optics letters*, 29(16):1876–1878, 2004.

[23] A. H. Safavi-Naeini, T. P. M. Alegre, J. Chan, M. Eichenfield, M. Winger, Q. Lin, J. T. Hill, D. E. Chang, and O. Painter. Electromagnetically induced transparency and slow light with optomechanics. *Nature*, 472:69–73, April 2011.

[24] J.J. Sakurai. *Modern Quantum Mechanics.* Addison-Wellsley, 2010.

[25] A. Schliesser, P. Del'Haye, N. Nooshi, K. J. Vahala, and T. J. Kippenberg. Radiation pressure cooling of a micromechanical oscillator using dynamical backaction. *Phys. Rev. Lett.*, 97:243905, Dec 2006.

[26] J. D. Teufel, T. Donner, D. Li, J. W. Harlow, M. S. Allman, K. Cicak, A. J. Sirois, J. D. Whittaker, K. W. Lehnert, and R. W. Simmonds. Sideband cooling of micromechanical motion to the quantum ground state. *Nature*, 475:359–363, July 2011.

[27] J. D. Teufel, J. W. Harlow, C. A. Regal, and K. W. Lehnert. Dynamical backaction of microwave fields on a nanomechanical oscillator. *Phys. Rev. Lett.*, 101:197203, Nov 2008.

[28] J. D. Thompson, B. M. Zwickl, A. M. Jayich, F. Marquardt, S. M. Girvin, and J. G. E. Harris. Strong dispersive coupling of a high-finesse cavity to a micromechanical membrane. *Nature*, 452:72–75, March 2008.

[29] D.F. Walls. *Quantum Optics.* Springer, 2008.

[30] Stefan Weis, Remi Riviere, Samuel DelÃľglise, Emanuel Gavartin, Olivier Arcizet, Albert Schliesser, and Tobias J. Kippenberg. Optomechanically induced transparency. *Science*, 330(6010):1520–1523, 2010.

[31] Christopher Wipf. *Toward Quantum Opto-Mechanics in a Gram-Scale Suspended Mirror Interferometer.* PhD thesis, MIT, 2013.